USING DIGITAL SPECTROSCOPY IN THE XRF MEASUREMENT OF Pb AND Hg

USING DIGITAL SPECTROSCOPY IN THE X-RAY FLUORESCENCE MEASURENT OF LEAD AND MERCURY

by

SANDRA N. BATEMAN, B.Sc., B.Ed.

A Thesis

Submitted to the School of Graduate Studies

in Partial Fulfillment of the Requirements

for the Degree

Master of Science

McMaster University

MASTER OF SCIENCE (2000)
(Physics and Astronomy)

McMaster University
Hamilton, Ontario

TITLE: Using Digital Spectroscopy in the X-ray Fluorescence Measurement of Lead and Mercury

AUTHOR: Sandra N. Bateman, B.Sc. (University of Guelph), B.Ed. (Brock University)

SUPERVISOR: Dr. David R. Chettle

NUMBER OF PAGES: viii, 84

ABSTRACT

X-ray fluorescence has been used to measure levels of lead in the bone for many years. This technique is particularly important for the occupational monitoring of those exposed to lead in the workplace as it provides an indication of long term exposure and retention in the body. The measurement of kidney mercury by x-ray fluorescence has been developed recently and is currently being improved for future use in occupational monitoring.

X-ray fluorescence detection systems conventionally employ analog-amplifier components. Recently, digital spectrometers have been developed which can replace these conventional electronics components. The digital systems offer higher throughput without major losses in resolution which translates to better precision and reduced detection limits for x-ray fluorescence measurements.

Investigations using the DSPECplus and DSA-2000 digital spectrometers for the measurement of bone lead in phantoms showed significant improvements in precision and potential reductions in MDL compared to conventional electronics. The use of the DSA-2000 digital spectrometer in a bone lead survey was shown to improve measurement uncertainties for *in vivo* bone lead measurements. Investigations using the DSA-2000 for the XRF measurement of kidney mercury in phantoms also showed a significant reduction in MDL for this system by the introduction of digital spectroscopy.

ACKNOWLEDGEMENTS

I would like to thank my supervisor Dr. David Chettle for his support, advice, and encouragement throughout the past two years. I would also like to thank my supervisory committee members for their work: Dr. Fiona McNeill, Dr. Bill Prestwich and Dr. Colin Webber.

I am very grateful to Dr. Ian Stronach for all of his help throughout this thesis; his knowledge, skills, and patience were very much appreciated. I also would like to thank Dr. Joanne O'Meara for introducing me to the kidney mercury system and always responding promptly and thoroughly to all of my questions (all the way from Bermuda). Marek Kiela also deserves thanks for his assistance on the kidney mercury system, and for his computer support throughout the past two years.

A special thank you goes to Michelle Arnold and Ana Pejović-Milić for not only helping me with many aspects of my research, but also for providing me with friendship and fun. I am grateful for the support and encouragement of Kathy, Barry, Lynn, Christine, and my parents. A very special thank you goes to Ian whose constant support is invaluable. A final thanks goes to Mollie and Sasquatch whose company during the typing of this thesis was very much appreciated.

TABLE OF CONTENTS

LIST OF FIGURES

LIST OF TABLES

Chapter 1

INTRODUCTION

1.1 Lead

1.1.1 Introduction

Due to its widespread use and vast distribution, lead is considered to pose a greater health and environmental hazard than any other element (Denny *et al.*, 1987). Lead has been used for over 3000 years and its toxic effects to humans have been known for over two centuries (Ratcliffe, 1981). The widespread use of lead has been due to its relative ease of extraction from its ore, its abundance in the earth's crust, and its malleability, resistance to corrosion, poor conductance, good sound absorption and good radiation absorption (Fergusson, 1990, Ratcliffe, 1981).

Ancient uses of lead included roofing, transport of water, storage of food and wine, cosmetics and pigments (Fergusson, 1990, Ratcliffe, 1981). Since the Industrial Revolution, lead has been mainly used in lead-acid storage batteries and as an anti-knock additive in gasoline (Fergusson, 1990). Lead is also used as a stabilizer in the plastics industry, ammunition, radiation shielding, plumbing, and paint additives, although the last two uses have declined in recent years due to increased awareness of lead's toxicity (Fergusson, 1990).

Inorganic lead is a more common environmental and occupational contaminant than organic lead, and, as a result, the majority of toxicology studies focus on the health effects of inorganic lead (Ratcliffe, 1981, Schwartz *et al.*, 1993).

1.1.2 Exposure and Retention in the Body

There are few areas on earth which are free of anthropogenic lead (Denny *et al.*, 1987). The levels of lead in the atmosphere in certain areas of the world are 1000 times what they were in pre-technological times (Denny *et al.*, 1987). The main sources of lead exposure are automobile emissions, paint pigments, smelting activities, waste incineration, lead pipes in older housing, and iron and steel production (Ratcliffe, 1981). The "dust vector" is the most important mode of transport for lead pollution, with the small size of the lead particles allowing them to be transported great distances through the air, and to be deposited on soil and water at distant locations (Denny *et al.*, 1987).

The main routes of exposure to lead for the general public are the inhalation of lead dust from the atmosphere, or ingestion of lead dust from food or water (Denny *et al.*, 1987). Atmospheric lead exposure is greater in urban areas with lead concentrations reaching 2 – 4 $\mu g/m^3$ air, while suburb and rural lead levels tend to be less than 0.2 $\mu g/m^3$ air (WHO, 1977). Lead levels in occupational settings have been greater than 1000 $\mu g/m^3$ air (WHO, 1977). Exposure from food is typically very small (~20 μg/day) with larger exposures resulting from the use of lead-containing storage or cooking vessels (WHO, 1977). The levels of lead in drinking water are also very low (less than 10 μg/l) unless lead pipes are being used in which case lead levels can reach 2000 – 3000 μg/l (WHO, 1977). Children often have a greater exposure level to lead than adults due to

their tendency to contact more lead dust playing in yards or streets, and to engage more frequently in hand-to-mouth activities (Fergusson, 1990). Another exposure route for children is by the exhibition of pica for lead-containing paint chips and other non-food items which can often taste sweet from the lead compounds they contain (Fergusson, 1990, WHO, 1977).

The amount of external dose of lead which is absorbed by the body depends on the intake method. 40 % of inhaled lead is deposited in the lungs, and 40 – 100 % of this lead is absorbed by the body, depending on the size of the particles (Fergusson, 1990). For adults, 10 % of the lead which is ingested is absorbed in the gastrointestinal tract (Hutton, 1987). For children this percent is higher, reaching up to 40 % for infants (Fergusson, 1990, Hutton, 1987).

Once absorbed by the body, the half-life of lead in the bloodstream is approximately one month (Skerfving *et al.*, 1993). The vast majority (over 90 %) of the lead in the body is stored in the skeleton with 70 % of this lead in the denser, cortical bones and with the remainder in the more "spongy" trabecular bones (Barry, 1975). The biological half-lives of lead in these two bone types have been estimated to be approximately 27 years and 16 years respectively (Gerhardsson *et al.*, 1993), although such estimates remain the subject of further work. In the bone, lead occupies the calcium position in the bone crystal and is biologically inactive (Ratcliffe, 1981) although it does serve as an endogenous lead source (Fergusson, 1990). The remaining lead in the body is mainly found in the teeth, kidney, liver and muscle (Barry & Mossman, 1970, Hutton, 1987, Ratcliffe, 1981).

The major excretion route of lead is through the urine (76 %), while 16 % is excreted through the gastrointestinal tract with the remainder excreted via sweat, hair and skin (WHO, 1977).

1.1.3 Health Effects

The toxicity of lead is classified as mid to high, with a daily tolerable intake of ~ 430 μg (Fergusson, 1990). Due to its vast use and wide distribution, lead is considered to be a dangerous toxin since it affects such a large population (Fergusson, 1990). It is a subclinical toxin which may not cause overt signs and symptoms at low level exposures, but can still cause physiological and biochemical changes at these levels (Hutton, 1987, Landrigan, 1989). The greatest concern for health effects from lead exposure are for those who are occupationally exposed and for children. Children are of special concern because not only does their exposure and uptake tend to be higher than that for adults, but their tolerance levels are also lower (Needleman, 1977).

Lead affects three main organ systems: the haematological system, the nervous system, and the nephrotic system (Hutton, 1987). Lead is also able to cross the placental barrier (Hutton, 1987). Clinical signs of high levels of lead exposure include anemia, wrist drop and renal failure, while subclinical effects of low level exposure include impaired heme biosynthesis, slowed nerve conduction, and altered uric acid excretion (Landrigan, 1989). Haematological system effects begin at blood lead levels of 10 – 20 μg/dl with the inhibition of the enzyme ALA-D (which is necessary for the synthesis of hemoglobin) (Landrigan, 1989), and result in anemia at blood lead levels greater than 50 μg/dl (Fergusson, 1990). Neurological effects begin at blood lead levels of 40 μg/dl with

reduced peripheral nerve conduction, and worsen to behavioural, psychological, intelligence, and visual-coordination changes at blood lead levels of 40 – 60 μg/dl (Fergusson, 1990). At blood lead levels greater than 100 μg/dl, encephalopathy can result (Fergusson, 1990). Renal effects begin with changes in the proximal tubule cells of the kidney at blood lead levels of 25 μg/dl (Landrigan, 1989), and advance to impaired kidney function at blood lead levels of 50 μg/dl (Fergusson, 1990).

1.1.4 Occupational Monitoring

Particularly due to its nature as a subclinical toxin, it is very important to monitor those who are occupationally exposed to lead. The major industries of concern include lead mining and smelting, lead battery production, and lead recycling. Threshold levels need to be set to protect workers from the negative health effects of long term lead exposure, and reliable monitoring processes are necessary to determine the workers' exposure levels.

Biological monitoring of occupationally exposed persons is an important procedure since physical monitoring of lead levels in the workplace environment can give only limited information. Biological monitoring takes into account different exposure sources and intake routes as well as individual variation in lead metabolism and past exposure (Skerfving *et al.*, 1987, 1993). Ideally, biologically monitoring should give an accurate reflection of total body burden so that the workers' exposure and risk can be properly assessed (Hu *et al.*, 1989).

The most common biological monitoring method for lead is the measurement of blood lead levels (Skerfving *et al.*, 1993). This method is easy and straightforward

(Skerfving *et al.*, 1993) but is only an indicator of recent exposure and can be affected by other factors such as endogenous lead sources (Fergusson, 1990, Skerfving *et al.*, 1987).

The enzyme ALA-D can also be measured as its levels are affected by lead exposure (Fergusson, 1990). However, this method is not very practical and the results are variable (Skerfving *et al.*, 1993).

Urine-lead levels are sometimes measured but these values give limited information due to high risk of contamination and variability in results (Skerfving *et al.*, 1993).

Mobilization tests can be performed using chelating agents such as EDTA or penicillamine to measure the amount of lead in the body. However, this method mainly measures the soft tissue lead content rather than that contained in the bone, resulting in limited information and variable results (Hu *et al.*, 1989).

Tissue biopsies can be performed to determine lead levels but this method is not desirable as it is invasive and involves risk to the worker (Börjesson & Mattsson, 1995).

Lead content of hair can be measured but there is a high probability of both endogenous and exogenous sources so that the measured value may not be an accurate reflection of the biological lead level (Fergusson, 1990).

The measurement of lead in the teeth can be used to give an indication of past lead exposure, but since this method uses deciduous teeth from children, its use is limited (Hu *et al.*, 1989, Fergusson, 1990).

The process of *in vivo* x-ray fluorescence can be used to measure the concentration of lead in the bone. This non-invasive, transportable method gives an accurate reflection of long term exposure and the results are indicative of total body burden of lead (Hu *et*

al., 1989, Skerfving *et al.*, 1993). This process is used today in occupational settings to monitor lead levels in the tibia, calcaneus and fingerbone (Skerfving *et al.*, 1993).

1.2 Mercury

1.2.1 Introduction

Mercury has been known since ancient times (Fergusson, 1990) and has been used in over 3000 applications in medicine and industry (D'Itri & D'Itri, 1977). Its toxic effects on the neurological system have also long been known, giving us expressions such as "mad as a hatter" based on the tremors and mood swings of those using $Hg(NO_3)_2$ to felt hats (Fergusson, 1990, Kaye, 1995), and the term "gibberish" based on the confused writings of the 8th century Arabian chemist Abu Jabiribnhayyan who is believed to have suffered from chronic mercury poisoning (Kaye, 1995).

Mercury has been used for the extraction of gold and silver, a medical treatment for syphilis, hat felting, a pigment for tattoos, fungicides for seeds, an antifungal additive for paint, and a slimicide for pulp and paper mills (Risher & DeWoskin, 1999). Currently, the main uses of mercury are in chloralkali cells, thermometers, electrical switches, batteries and dental amalgams (Fergusson, 1990, OML, 1986).

1.2.1 Exposure and Retention in the Body

The contribution to mercury in the atmosphere from man-made sources is approximately the same as the contribution from natural processes such as the breakdown of minerals by wind and water, and by volcanic activity (Risher & DeWoskin, 1999). 80 % of the mercury released from human sources is as elemental mercury released into the atmosphere from fossil fuel combustion, mining, smelting, and solid waste

incineration (Risher & DeWoskin, 1999). 15 % is released to the soil from fertilizers, fungicides and municipal solid waste, while the remaining 5 % is released into the water from industrial wastewater (Risher & DeWoskin, 1999). The easiest mode of transport for mercury is as mercury vapour, and due to its long residence time in the atmosphere, it can travel for great distances (Goldberg & Wren, 1987, Vostal, 1972).

The major routes of exposure to mercury for the general population are the ingestion of methylmercury from fish, the inhalation of mercury vapour from dental amalgams, and the inhalation of mercury vapour from the atmosphere (Risher & DeWoskin, 1999). However, for the average person, the exposure from these sources is well below what is considered to be a "safe" limit. Urban outdoor air concentrations range from 10 – 20 ng Hg/m^3, an average mercury intake through food per day is ~ 3.5 μg, and typical releases from mercury amalgams range from 3 – 17 μg Hg per day depending on the number of fillings (Risher & DeWoskin, 1999).

The amount of external mercury dose which is absorbed by the body depends on both the form of the mercury and the intake method. For elemental mercury, approximately 80 % of inhaled mercury is absorbed into the bloodstream, while less than 0.01 % of ingested mercury will be absorbed in the gastrointestinal tract (Friberg & Nordberg, 1973, Nordberg & Skerfving, 1972). For inorganic mercury salts, inhalation is not a main uptake route, and the absorption fraction depends on the size of the particles (Nordberg & Skerfving, 1972, Risher & DeWoskin, 1999). When swallowed, the amount of absorption of mercury salts in the gastrointestinal tract ranges from 10 – 40 % depending on the solubility of the compound (Nordberg & Skerfving, 1972, Risher &

DeWoskin, 1999). There is also a small amount of uptake through the skin for inorganic mercury salts (Risher & DeWoskin, 1999). The main route of uptake for organic mercury compounds, such as methylmercury, is by ingestion where there is almost complete absorption in the gastrointestinal tract (Nordberg & Skerfving, 1972). There is also evidence of uptake through the skin (especially for dimethylmercury) and transplacental transfer (Risher & DeWoskin, 1999).

Once absorbed in the body, inorganic mercury concentrates mainly in the kidney, with the liver, spleen and brain also showing elevated mercury levels (Matsuo *et al.*, 1989, Nordberg & Skerfving, 1972). The biological half-life in the body is approximately 1 – 2 months (Nordberg & Skerfving, 1972). Excretion is mainly through the urine or feces with a small amount excreted via the lungs, sweating and lactation (Nordberg & Skerfving, 1972). Methylmercury mainly concentrates in the brain with some retention in the liver and kidneys as well (Hutton, 1987). The biological half-life is approximately 2 – 3 months (Nordberg & Skerfving, 1972). Excretion of methylmercury is via the feces, mainly as inorganic mercury (Risher & DeWoskin, 1999).

1.2.3 Health Effects

Mercury is classified as an extremely toxic element with a tolerable intake of 40 μg/day (Fergusson, 1990). The effects on the body are mainly on the kidney and nervous system with the type and extent of damage depending on the specific form of mercury absorbed.

Exposure to elemental mercury vapour mainly leads to nervous system disturbances, tremors, lung damage, nausea, vomiting and kidney damage (OML, 1986, Risher &

DeWoskin, 1999). Exposure to inorganic mercury salts can result in gastrointestinal damage, skin burns, nervous system effects, tremors, loose teeth, sore gums, headache, fatigue, and kidney damage (D'Itri & D'Itri, 1977, OML, 1986, Risher & DeWoskin, 1999). Organic mercury compounds have the most destructive effects on humans (Fergusson, 1990). Several large outbreaks of organic mercury poisonings have occurred in the past such as the methylmercury poisoning from fish in Minamata Bay in the 1950's and 1960's, and the poisoning of hundreds of people in Iraq in the 1970's from flour grains dressed in mercury-based fungicide (Hutton, 1987). Exposure to methylmercury can result in loss of sensation around the mouth, loss of coordination, loss of hearing, restricted visual field, involuntary movement, mental disturbances, excess salivation, permanent kidney and brain damage, and damage to the fetus (Fergusson, 1990, Risher & DeWoskin, 1999, Skerfving & Vostal, 1972). There is a latent period of several weeks or months between the uptake of methylmercury and the appearance of symptoms while the mercury accumulates in the body which adds to the dangerous nature of this compound (Fergusson, 1990). Dimethylmercury is another extremely dangerous organic mercury compound. A chemistry professor recently died after an accidental transdermal exposure to a few drops of dimethylmercury (Nierenberg *et al.*, 1998). The autopsy revealed brain damage to the cerebral cortex area similar to that found from methylmercury poisoning (Nierenberg *et al.*, 1998).

The initial symptoms of mercury poisoning begin at blood mercury levels of 1 – 10 μg/dl, with increased nervous system effects at levels greater than ~12 μg/dl (Risher & DeWoskin, 1999). A fatal blood mercury level is greater than 140 μg/dl (Fergusson,

1990). Normal blood mercury levels range from < 0.5 to 2 μg/dl (Risher & DeWoskin, 1999).

1.2.4 Occupational Monitoring

As was the case with lead, it is very important to have reliable procedures to monitor the exposure levels for those occupationally exposed to mercury. The main industries of concern include chloralkali plants, thermometer factories, alkaline battery factories and the dental amalgam industry. It is particularly important to monitor the exposure level of workers because, in most cases, they appear to be in good health, and therefore alternative indicators of exposure are needed (Smith *et al.*, 1970).

Physical monitoring of the mercury concentration in the workplace air is commonly performed but this is not an ideal method of estimating occupational exposure. It does not account for variations in work activities, different sources and intake routes, individual variation in metabolism, or past exposure (Langworth *et al.*, 1991, Skerfving *et al.*, 1987). Variations in air-Hg readings also occur depending on the type of sampling device used (Sällsten *et al.*, 1992). Daily air-Hg levels have been found to correlate with daily blood and urine levels (Roels *et al.*, 1987), but physical monitoring still offers more limited information than biological monitoring. A biological monitoring technique that estimates total body burden would be the most useful for assessing workers' exposure and risk.

Occupational exposure is often monitored by measuring mercury levels in the urine (U-Hg) but this technique is not useful for determining methylmercury exposure since most of the excretion of this compound is via the feces (Langworth *et al.*, 1991). The

main use of U-Hg is for monitoring inorganic mercury exposure although this method gives variable results and is useful only once a steady state of exposure has been reached (OML, 1986, Piotrowski *et al.*, 1975).

Measuring the mercury content of the blood (B-Hg) can be used to determine inorganic and methylmercury levels (Risher & DeWoskin, 1999). This measurement, however, reflects very recent, rather than chronic, exposure (Barregård, 1993). One of the main obstacles with the B-Hg measurement is that mercury exposure from fish consumption and dental amalgam surfaces greatly affects the B-Hg levels, decreasing this method's sensitivity (Barregård, 1993, Sällsten *et al.*, 1990). For example, a study on dental workers showed that the exposure from their own dental amalgams was approximately equal to their occupational exposure (Akesson *et al.*, 1991).

Levels of mercury in hair can be measured but this process is unreliable due to the high risk of external contamination (Nordberg & Skerfving, 1972). Breath vapour levels can be measured within a few days of exposure, but these levels are only indicative of short term exposure (Risher & DeWoskin, 1999).

Recently, *in vivo* x-ray fluorescence has been used to measure levels of mercury in the kidney (Börjesson *et al.*, 1995). Since the kidney is the main organ of mercury retention, the measurement of mercury concentration in the kidney would be valuable in determining the mercury body burden. There is ongoing work in this area to improve the measurement system and to allow for further occupational monitoring and mercury metabolism studies in the future.

1.3 X-ray Fluorescence

1.3.1 Background Theory: Photon Interactions

X-ray fluorescence (XRF) is the emission of characteristic x-rays from a target element via the photoelectric effect. The target element can be excited by photons emitted from a radionuclide source or from an x-ray tube. Besides the photoelectric process, two other main interactions occur between photons and matter: Compton scattering and coherent scattering. These three processes will be described below.

a) The Photoelectric Effect

The photoelectric effect occurs when a photon interacts with one of the tightly bound electrons in an atom. The photon transfers all of its energy to the electron which is then ejected from the atom. The vacancy which now exists in the inner shell is filled by an electron from one of the outer shells of the atom. To compensate for the resulting decrease in potential energy of this electron, an x-ray is emitted from the atom. Alternatively, an electron from one of the outer shells can be ejected instead of an x-ray, which is known as Auger emission. A diagram of the photoelectric process is shown in figure 1.1.

The x-rays which are emitted by an atom are said to be "characteristic" in that their energies are unique to that element. The shells of each atom are labelled K, L, M, etc. starting from the inner shell. In order for the photoelectric process to occur, the incoming photon must have an energy greater than the binding energy of the electron to be ejected. 80 % of all photoelectric interactions are a result of the ejection of a K-shell electron (providing the incoming photon has an energy greater than the K shell binding energy).

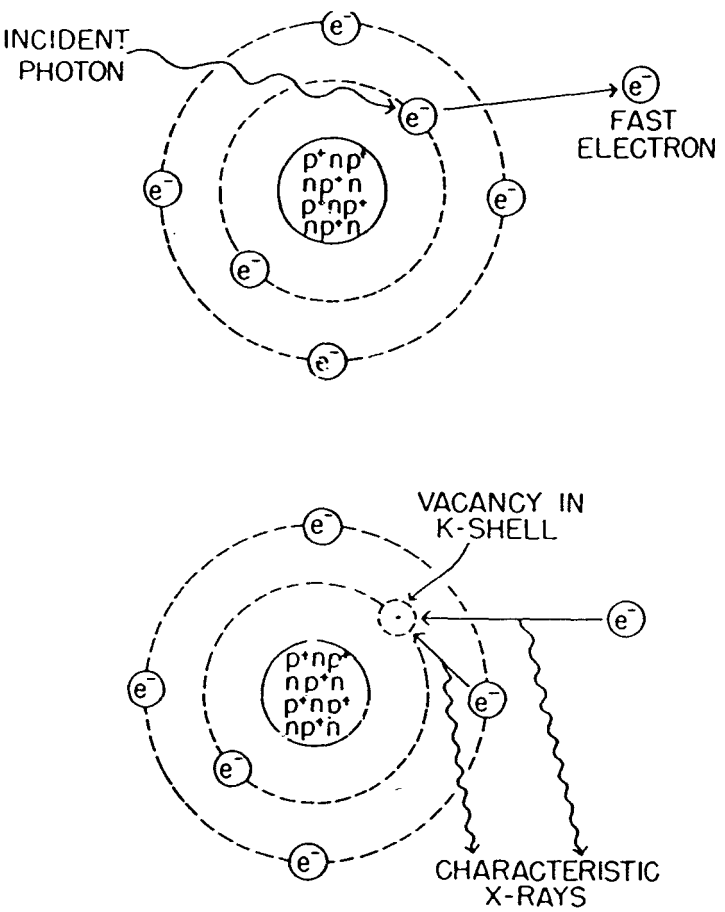

Figure 1.1 The Photoelectric Effect (Hall, 1994)

The x-rays emitted from this type of interaction are called K x-rays. X-rays emitted from the ejection of an L-shell electron are called L x-rays, and so on. When a K-shell vacancy is filled by an L-shell electron, the emitted x-ray is called a K_α x-ray and its energy is equal to the energy difference between the K- and L-shell binding energies. If the vacancy is filled by an M-shell, or higher shell, electron, the x-ray is called a K_β x-ray, and its energy is equal to the energy difference between the K-shell and higher shell binding energies. X-ray sublevels also occur due to the existence of subshells in the atom. For example, the $K_{\alpha 1}$ x-ray results from the transition of an L_{111}-shell electron to a K-shell vacancy.

b) Compton Scattering

Compton, or incoherent, scattering is the inelastic scattering of a photon from an atom. The original photon is deflected and transfers some of its energy to a recoil electron. The final energy of the photon (E_γ') is given by the following equation:

$$E_\gamma' = E_\gamma / [\, 1 + \alpha\,(1 - \cos\theta)\,] \qquad [1.1]$$

where $\alpha = E_\gamma / mc^2$, E_γ is the initial energy of the photon, θ is the angle of scatter, and mc^2 is the rest mass energy of the electron. Compton scattering offers little information for the *in vivo* XRF analysis of tissues, yet unfortunately is often a dominant spectral feature. Geometry and source energy considerations are important in order to minimize the Compton scattering contribution in XRF analysis.

c) Coherent Scattering

Coherent scattering is the elastic scattering of a photon from an atom, and results in the emission of a photon with unchanged energy. It is a generalization of Thompson

scattering, the classical interaction between a photon and an electron, where each electron in the atom acts as a scattering centre. The overall process can be thought of as the superposition of the effects from each scattering centre.

The cross section for coherent scattering is shown below:

$$d\sigma = \tfrac{1}{2} r^2 (1 + \cos^2\theta) \, | F(K)^2 |^2 \, d\Omega \qquad [1.2]$$

where r is the classical electron radius, θ is the angle of scatter, and F(K) is the atomic form factor, which is a function of atomic number, Z, photon energy, E, and θ. At large scattering angles, the cross section varies by Z^5 or Z^6, and therefore the major source of coherently scattered photons at these angles are high Z elements. This is a very important factor in the normalization procedure for determining lead concentration in the bone, which will be discussed in the next section.

1.3.2 Source Excited XRF – The Bone Lead Detection System

The *in vivo* XRF measurement of bone lead is generally done using a radionuclide source for the excitation of the lead atoms. The first XRF bone lead measurements were reported in 1976 using a Co-57 source in a 90° scattering geometry (Ahlgren *et al.*, 1976). These measurements were done on the tibia and fingerbone and were based on the emission of K x-rays. Since this time, several variations and improvements on this system have been developed. For example, I-125 has been used as a photon source in a system which detects L x-rays in the tibia (Wielopolski, 1983), Cd-109 is used in a K x-ray detection system which measures lead in the tibia or calcaneus (Somervaille *et al.*, 1985, Fleming *et al.*, 1997), and polarized x-rays have been used in the measurement of L x-rays from the tibia (Wielopolski *et al.*, 1989).

There are several factors to consider when determining which detection system set-up to use. One of the most important factors is penetration into, and out of, the bone measurement site, which is dependent on the γ- and x-ray energies. The energies of the K and L x-rays for lead are listed in the table below.

X-ray	$L_{\alpha 1}$	$L_{\beta 1}$	$K_{\alpha 2}$	$K_{\alpha 1}$	$K_{\beta 1}$	$K_{\beta 2}$	$K_{\beta 3}$
Energy (keV)	10.549	12.611	72.804	74.969	84.936	87.300	84.450

Table 1.1 Energies of lead L and K x-rays (Lederer & Shirley, 1978)

The attenuation mean free paths for 11.5 and 75 keV photons in bone are 0.028 and 2.2 cm respectively, while the corresponding values for soft tissue are 0.31 and 5.4 cm (Somervaille *et al.*, 1985). Due to their higher attenuation in bone and soft tissue, L x-rays can only be used for superficial bone measurements, while K x-rays can be used for measurements over much larger depths, and therefore much larger bone volumes (Hu *et al.*, 1989).

There are several factors to consider when choosing a bone measurement site. It is desirable to have a site which is easily accessible, large in volume, located far away from radiosensitive organs, and representative of total skeletal body burden (Hu *et al.*, 1989). The tibia is frequently the bone site of choice in that it fulfills the above criteria. The calcaneus and patella are suitable sites for measuring lead concentrations in trabecular bone, which can then be compared to lead concentrations found in the cortical bone of the tibia (Hu *et al.*, 1989).

The choice of photon source is affected by the fluorescence yield per incident photon and by the amount of background under the lead x-rays due to Compton

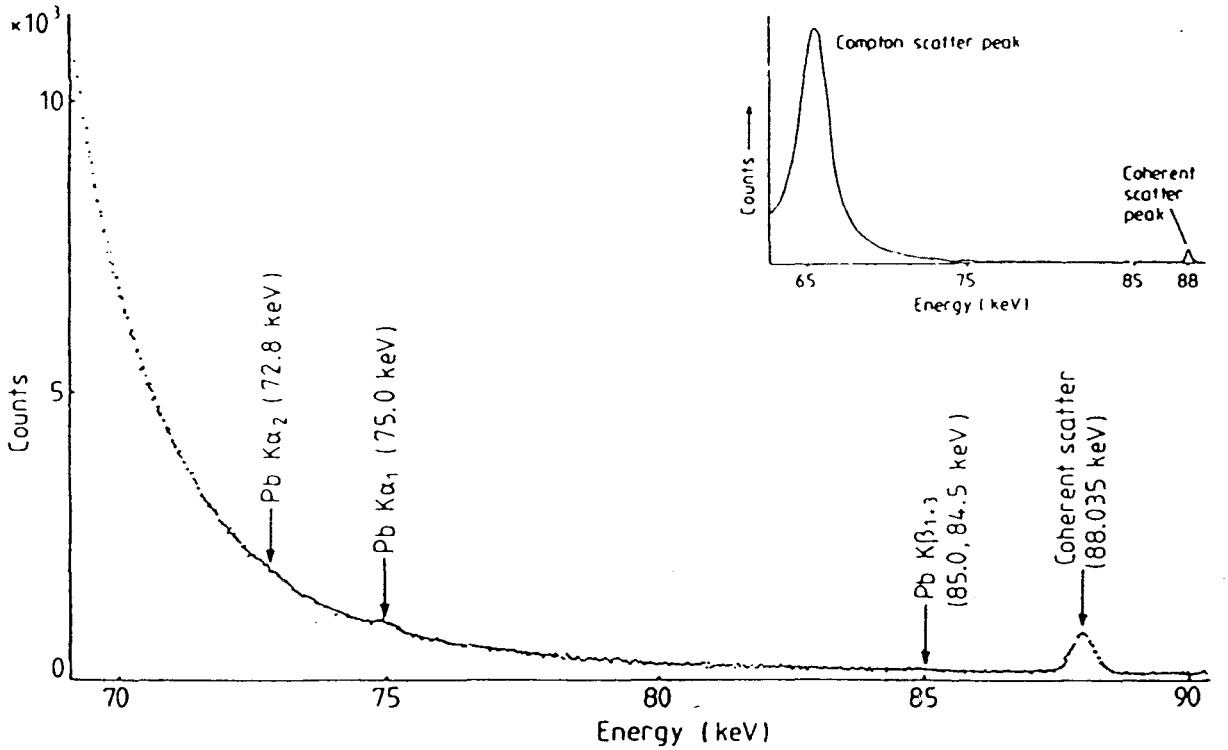

Figure 1.2 Typical Lead XRF Spectrum (Somervaille *et al.*, 1985)

scattering. Cd-109 has an extremely high fluorescence yield/incident photon since it emits γ-rays of energy 88.035 keV, which is just above the K-edge of lead at 88.005 keV (Somervaille *et al.*, 1985). As can be seen from figure 1.2, the Compton scatter peak is a very dominant feature of the lead XRF spectrum. To minimize the Compton background under the lead x-rays, photon energies and source-sample-detector geometry must be considered. Comparisons of the positions of the Compton scatter peak for Cd-109 and Co-57 sources, and for 90° and 180° geometries are shown in table 1.2 below.

Source	Principal γ-ray Energy (keV)	Energy of main Compton peak (keV) 90 ° geometry	Energy of main Compton peak (keV) 180 ° geometry
Cd-109	88	75	65
Co-57	122, 136	98, 107	83, 89

Table 1.2 Energies of main Compton peaks for differing sources and geometries. (Somervaille *et al.*, 1985)

It can be seen from table 1.2 that the best combination for background reduction is a Cd-109 source in a backscatter (180°) geometry since this will result in a Compton scatter peak that is furthest from, and below, the lead K x-rays (which range from ~ 72 keV - 87 keV). While Co-57 in a 90° geometry also offers good separation between the Compton peak and lead x-rays, the photoelectron absorption cross section for lead is lower for Co-57 (2.82 cm^2/g) than for Cd-109 (7.37 cm^2/g) (Somervaille *et al.*, 1985).

The sizes of the lead x-ray peaks in the spectrum depend not only on the concentration of lead in the bone, but also on the thickness of the overlying tissue, the shape and size of the bone, and the distance between the source and the sample (Somervaille *et al.*, 1985). These factors are not easy to correct for, and would make the bone lead concentration difficult to determine accurately. However, a technique has been

developed for the Cd-109 backscatter geometry system which normalizes the lead K x-ray peaks to the coherent scatter peak, and makes the above corrections unnecessary (Somervaille *et al.*, 1985). This normalization technique will be described below.

For photon energies of ~ 88 keV (that of the Cd-109 γ-rays) and scattering angles of ~ 150° (the mean scatter angle for the backscatter geometry), the coherent scatter cross section varies as Z^5 or Z^6 (Chettle *et al.*, 1991). As a result, approximately 99 % of the coherent scatter signal in the lead XRF spectrum is due to the high Z bone mineral elements, as opposed to the low Z elements in the soft tissue surrounding the bone (Chettle *et al.*, 1991). The lead K x-ray signals can essentially be considered to be the result of interactions with unscattered photons, since only photons which have been Compton scattered through less than 3.6° will be left with an energy greater than the K-edge of lead, and this fraction is negligibly small (Somervaille *et al.*, 1985). As a result, both the coherent scatter signal and the lead K x-ray signals are due to the same flux of Cd-109 γ-rays. This allows for the normalization of the lead x-ray signals to the coherent scatter signal, which can be translated to a ratio of lead / bone mineral, independent of bone size and shape, overlying tissue thickness and sample-source distance (Somervaille *et al.*, 1985).

In order to determine the concentration of lead per gram of bone mineral, a calibration is performed using a set of plaster of Paris phantoms doped with known amounts of lead. A correction is made to account for the difference between the coherent scattering cross sections for plaster of Paris and bone (Chettle *et al.*, 1991). The results

of this normalization technique have been compared to atomic absorption spectroscopy analysis and have been found to be very accurate (Chettle *et al.*, 1991).

The McMaster University *in vivo* XRF system detects lead K x-rays from the tibia and calcaneus using a Cd-109 source in a backscatter geometry. As a result, the normalization technique described above is able to be used to determine bone lead concentrations per gram of bone mineral. In order to analyze the spectral results, fitting routines based on the Marquardt nonlinear least-squares method are used (Marquardt, 1963). The spectrum is divided into three sections for anaylsis: $K_{\alpha 2}$ and $K_{\alpha 1}$, $K_{\beta 1}$ and $K_{\beta 3}$, and $K_{\beta 2}$ and the coherent peak. Initially, the coherent scatter peak is fit to a Gaussian function, with the determined width and height used for the remaining analyses. The first two sections are fit with double exponential background functions, and the third section is fit with a single exponential background function. The fitting routine also takes into account the Ca edge at 84.0 keV which is the upper end of the doppler broadened spectrum from Compton scattering off the K-shell electrons of calcium (O'Meara, 1999). As well, a "complementary error function" is included in the fitting routine to account for the "step" seen in the low-energy end of the Gaussian peaks due to incomplete charge collection in the detector.

Bone lead measurements are typically 30 minutes in length and result in an effective whole body dose of approximately 30 - 40 nSv. This is comparable to the natural background radiation dose received in 5 - 10 minutes assuming an annual level of 2 - 3 mSv (Todd *et al.*, 1992). A typical measurement precision is 3 μg lead/g bone mineral,

which translates to a minimum detection limit (MDL) of 6 μg lead/g bone mineral (defining the MDL as twice the measurement uncertainty) (Gordon *et al.*, 1993).

1.3.3 Polarized XRF – The Kidney Mercury Detection System

In vivo measurements of kidney mercury have recently been made using plane polarized x-ray fluorescence (Börjesson *et al.*, 1995). Previously, attempts were made to measure bone mercury levels using Co-57 source-excited systems (Bloch & Shapiro, 1981, Skerfving *et al.*, 1987). However, these methods were not promising since mercury is not a bone seeker and levels were often too low to detect, and also not representative of mercury body burden. Although the kidney was the best choice for a measurement site, it was initially thought that XRF would not be a reliable technique for this measurement. The depth of the kidney in the body (3 – 5 cm) allows for large amounts of scatter and attenuation, and degrades the signal-to-noise ratio (Bloch & Shapiro, 1981). Studies on the Co-57 XRF system using kidney phantoms showed that the measurement of occupationally exposed workers may be feasible, but in order to measure lower levels, improvements to the system must be made (Smith *et al.*, 1982).

The use of plane polarized x-ray fluorescence was a solution to the problem of measuring mercury in the kidney. A reduction in background counts of ~ 60 % is produced by using this technique (Börjesson *et al.*, 1995). The photons are polarized by Compton scattering from a low Z material. Since this scattering process can reduce the photon fluence by a factor of ~ 10^4, x-ray tubes are used instead of radionuclide sources to provide a high intensity beam of photons (Christoffersson & Mattsson, 1983).

The primary beam polarization and subsequent reduction in background counts are

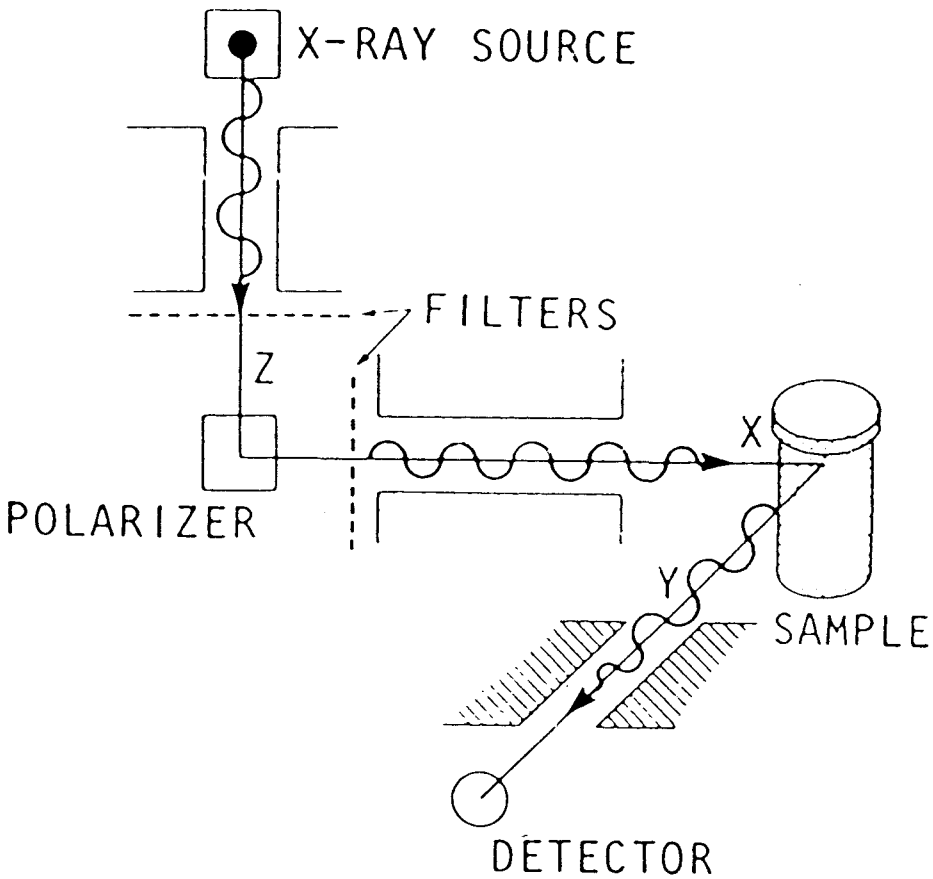

Figure 1.3: Physical Arrangement of Source, Polarizer, Sample and Detector for Polarized X-ray Fluorescence Measurement (Kaufman & Camp, 1974)

achieved by positioning the three beam paths (x-ray tube to polarizer, polarizer to sample, and sample to detector) in appropriate directions. Figure 1.3 shows a diagram of this set-up. The cross section for Compton scattering for polarized radiation is shown below:

$$d\sigma = \tfrac{1}{2} r^2 (\upsilon'/\upsilon)^2 [(\upsilon/\upsilon') + (\upsilon'/\upsilon) - 2 \sin^2\theta \cos^2\xi] d\Omega \qquad [1.3]$$

where r is the classical electron radius, θ is the angle of scatter, υ is the frequency of the incoming photon, υ' is the frequency of the scattered photon, and ξ is the angle between the plane of polarization of the incoming photons and the scattering plane. The cross section is minimized when θ is 90° and ξ is 0°. Referring to figure 1.3, it can be seen that the source, polarizer and sample are positioned such that the primary, unpolarized beam is Compton scattered through 90° towards the sample, and has been plane-polarized in the x-y plane. The detector has been positioned in the same plane as the polarization plane (the x-y plane) since the polarized photons cannot Compton scatter 90° back into their plane of polarization (Kaufman & Camp, 1974). The Compton scattering in this plane is not completely reduced to zero since multiple scattering (in both the polarizer and sample) and the non-zero solid angle affect the degree of polarization (Dzubay *et al.*, 1974).

The *in vivo* XRF mercury kidney system developed by Börjesson *et al.* (1995) measured the K series x-rays from mercury using a 160 kV (20 mA) x-ray tube photon source and an aluminum polarizer. The system employed a high-purity planar germanium detector (32 mm diameter, 10 mm thick) with a charge sensitive preamplifier, linear amplifier (shaping time 1.5 μs), and successive approximation ADC (fixed

conversion time 1.5 μs). Figure 1.4 shows a typical mercury XRF spectrum. The energies of the mercury K x-rays are shown in table 1.3 below.

X-ray	$K_{\alpha 2}$	$K_{\alpha 1}$	$K_{\beta 1}$	$K_{\beta 2}$
Energy (keV)	68.895	70.819	80.2	82.5

Table 1.3 Energies of mercury K x-rays (Lederer & Shirley, 1978)

The choice of voltage for the x-ray tube is dependent on the absorption edge of the element being excited. The K-edge for mercury is 83.103 keV. In order to have an energy of ~ 83 keV after polarization, a primary photon energy of greater than 99 keV is necessary (Börjesson, 1996). The 160 kVp tube voltage used satisfied this criterion.

A 0.35 mm thick uranium filter was placed between the polarizer and the subject to reduce the amount of low energy photons, and therefore the absorbed dose, to the patient (Börjesson *et al.*, 1995). Calibration phantoms containing known amounts of mercury were used for the determination of mercury concentrations in the kidney. The phantoms were placed at specific positions during measurements, which could then later be correlated with the position of the kidney in the patient, which was determined by ultrasound (Börjesson *et al.*, 1995). A 50 minute measurement time resulted in an effective dose of 0.03 mSv, and MDL's ranging from 12 to 45 μg/g (mean value 26 μg/g) depending on kidney depth (Börjesson *et al.*, 1995). A suggestion was made that increasing the x-ray tube potential might decrease the MDL, an investigation which was subsequently carried out at McMaster University by O'Meara in 1999.

The McMaster University polarized XRF system was optimized for mercury measurements by O'Meara (1999). The optimized system used a 1 cm thick aluminum

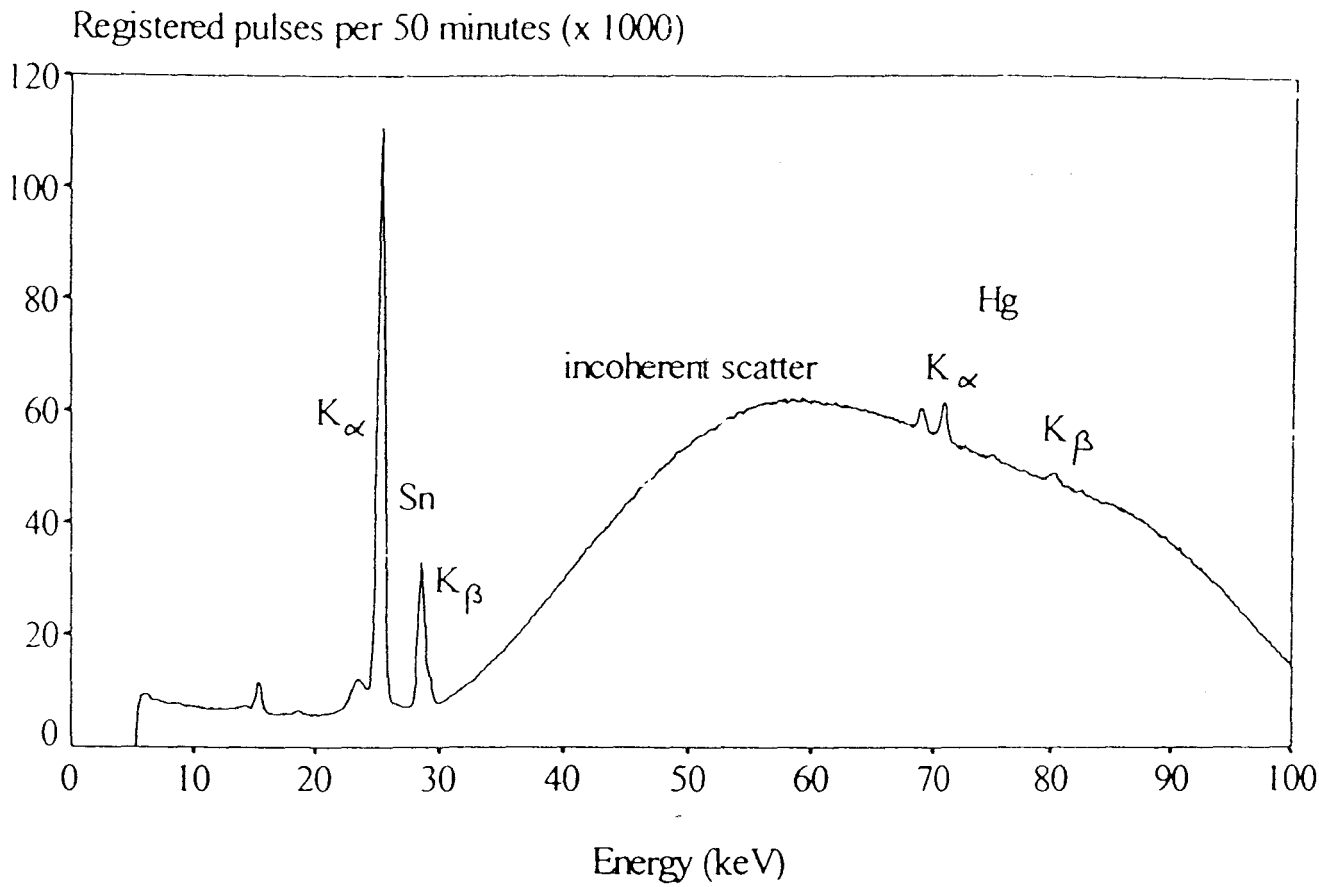

Figure 1.4 Typical Mercury XRF Spectrum. (Börjesson, 1996)
Note: The Sn peaks are due to Sn in the collimator.

polarizer and a 1.6 mm titanium filter placed between the x-ray tube and the polarizer. The effect of increasing x-ray tube voltage on the MDL was tested. Tube potentials of 250 kVp and 175 kVp (with current ~ 12.5 mA) were both used to make kidney phantom measurements at different positions. The analysis of the spectra was done using the Marquardt method of nonlinear least-squares (Marquardt, 1963). The spectra were analysed in three sections: $K_{\alpha 2}$, $K_{\alpha 1}$, and $K_{\beta 1,3}$. Each section was fit with a single exponential background, with the α sections each being fit with single Gaussian peaks, and the β section fit with two Gaussians (O'Meara, 1999).

Results of the MDL calculations for two of the positions are shown in table 1.4 below.

Location of Phantom	MDL for 175 kVp	MDL for 250 kVp
2 cm (lateral), 5 cm (dorsal)	39 +/- 4 ppm	26 +/- 1 ppm
6 cm (lateral), 5 cm (dorsal)	86 +/- 12 ppm	54 +/- 6 ppm

Table 1.4 Detection limits found for differing x-ray tube voltages (O'Meara, 1999)

It can be seen from table 1.4 that the increase in tube potential results in a significant reduction in MDL. The associated effective dose for a 30 minute measurement using a 250 kVp tube potential was determined to be 7 μSv (O'Meara, 1999). There is ongoing work in this area to further improve the signal-to-noise ratio, and therefore reduce the MDL, for the *in vivo* XRF kidney mercury detection system.

Chapter 2

SPECTROSCOPY SYSTEMS

2.1 Introduction

In order to detect and quantify the photons of differing energies emitted in the x-ray fluorescence technique, a gamma-ray spectroscopy system is used. The main components of a spectroscopy system are a detector, preamplifier, amplifier, analog-to-digital converter (ADC), and multichannel analyzer (MCA). New digital spectroscopy systems have recently been introduced which replace the amplifier and ADC components of a conventional electronics system. The basic components of the conventional and digital spectroscopy systems will be discussed in the following sections.

2.2 Basic Components

a) Detector

High-purity germanium (HpGe) detectors are used in the McMaster University lead and mercury XRF systems. A HpGe detector is a semiconductor device which is operated under a reverse bias. Incoming ionizing radiation creates charge carriers (electron/hole pairs) in the germanium crystal which are collected as a current pulse by the applied electric field. The amount of charge created in the crystal is proportional to the energy of the incident radiation.

The area of the germanium crystal which is sensitive to radiation is known as the depletion region. This area occurs at the p-n junction of the semiconductor where a charge imbalance exists due to the net diffusion of conduction electrons to the p side, and holes to the n side, which eventually creates an electric field that inhibits further diffusion. This junction area is now greatly "depleted" of holes and conduction electrons, and will therefore carry no current in the absence of ionizing radiation. Any charge which is created here will be swept away from the junction to the n or the p side as a current pulse. The application of a reverse bias voltage enhances the natural potential difference across the junction, and further prevents the diffusion of electrons and holes (i.e. current) without the presence of ionizing radiation, effectively increasing the size of the depletion region. The creation of charge by thermal excitation is suppressed by cooling of the crystal with liquid nitrogen.

The McMaster University lead XRF system uses a Canberra high purity germanium detector (model GL2020R) with an active face area of 2000 mm^2 and a thickness of 20 mm, operated at a voltage of – 2500 V. The mercury XRF system uses a Princeton Gamma-Tech high purity germanium detector (model NIGP 2020) with an active face area of 2000 mm^2, thickness of 20 mm, and operating voltage of – 2500 V.

b) Preamplifier

The amount of charge created within HpGe detectors is extremely small and is impractical to work with directly. The purpose of the preamplifier is to amplify this signal so that it can be further processed. Charge-sensitive preamplifiers are commonly used with semiconductor detectors, and give an output voltage which is proportional to

the total integrated charge in the pulse. The output signal of the preamplifier is a linear tail pulse with a relatively short rise time, but a relatively long decay time, so that full charge collection can occur for detectors with pulses of widely varying collection times. One disadvantage to this long tail pulse is that pulse pileup readily occurs. When a pulse rides on the tail of a previous pulse, it is possible for the combined voltage of the pulses to exceed the threshold of the preamplifier and cause saturation. This can lead to distortion of the pulses and resolution degradation. Saturation occurs more easily for high count rate and high energy situations.

The McMaster University lead XRF system uses a Canberra charge-sensitive preamplifier (model 2001CP) while the mercury XRF system uses a Princeton Gamma-Tech charge-sensitive preamplifier (model RG15B/C).

c) Amplifier

The main purpose of the amplifier is to amplify and shape the signal from the preamplifier. CR and RC circuits are used for pulse shaping. The output signal from the preamplifier is first shaped by a CR differentiator, or high pass filter, which "differentiates away" the long tail and filters out the low frequency noise (Knoll, 1989). This output is then shaped by RC integrators, or low pass filters, which results in a Gaussian shaped output pulse with the high frequency noise filtered out. The amplitude of the Gaussian pulse is proportional to the voltage input from the preamplifier.

The choice of time constants for the amplifier pulse shaping is based on a number of compromises. A short time constant reduces pulse pileup and baseline shift, but causes poor resolution from the effect of ballistic deficit. Ballistic deficit occurs when the full

amplitude of a shaped pulse is not reached because the amplifier time constant chosen is too short. Larger time constants reduce ballistic deficit and improve resolution, but will then increase pulse pileup and baseline shift. The time constant chosen for a particular application is one which results in an acceptable trade-off between throughput and resolution.

The McMaster University lead and mercury XRF systems both use a Canberra fast spectroscopy amplifier (model 2024) with a time constant of 1.0 μs.

d) Analog-to-Digital Converter

The linear output pulse from the amplifier is converted to a binary word by the analog-to-digital converter (ADC). The value of the digital output is proportional to the amplitude of the input pulse. The linear ramp converter ADC is commonly used in gamma-ray spectroscopy. Although it is slower than other ADC types, it offers excellent linearity. The Wilkinson-type linear ramp converter works by comparing the amplitude of the input pulse with that of a linearly increasing ramp voltage generated by charging a capacitor. The comparison is carried out by a ramp comparator circuit which sends a gate pulse to a linear gate which remains open for the time it takes the ramp to reach the input pulse amplitude. A constant frequency clock sends pulses to the linear gate during this "open" time, and the number of these pulses is counted by an address register. The digital output of the ADC is derived from the number of pulses counted by the register. This value is proportional to the time the linear gate is open, and is therefore also proportional to the amplitude of the input pulse.

The McMaster University lead and mercury XRF systems both use a Canberra 450 MHz Wilkinson-type ADC (model 8077).

e) Multichannel Analyzer

The purpose of the multichannel analyzer (MCA) is to store and display the digital information from the ADC. Each value from the ADC is stored in an appropriate channel and the resulting display is a plot of channel content versus channel number (a differential pulse height distribution). Once calibrated, this plot becomes an energy distribution spectrum.

The McMaster University lead XRF system uses a Canberra S100 MCA system while the mercury XRF system uses a Canberra Accuspec MCA system.

2.3 Digital Signal Processing

Digital spectroscopy systems differ from conventional electronics systems mainly in the amplifier and ADC stages. Unlike conventional systems, the digital systems first use an ADC to digitize the preamplifier output, and then shape this digitized signal with a digital filter. The detector and preamplifier components can be the same as for conventional systems, although the digital systems generally have their own MCA components.

The crucial difference between digital and conventional spectroscopy systems is in the signal filtering. The best signal-to-noise ratio can be achieved by using an infinite cusp pulse shape (Knoll, 1989). Since this shape would be impractical to deal with, a cusp with a finite width would be the ideal shape for practical purposes. However, this pulse shape is very difficult to achieve using the analog electronics of conventional

systems. Digital systems, however, can use digital processing algorithms to generate flat top cusp or trapezoidal pulse shapes which offer superior signal-to-noise ratios and reduced ballistic deficit. The main advantage of these systems is a much higher throughput potential without significant losses in resolution, which is particularly important for high count rate situations. Other advantages of digital spectroscopy include the large selection of shaping times available to suit different applications, and increased stability with temperature and time.

The specific components of two digital spectrometers, the DSPECplus and the DSA-2000, will be discussed below.

2.3.1 DSPECplus

The DSPECplus is the second generation digital spectrometer introduced by PerkinElmer (formerly EG&G ORTEC) in 1999. The first generation DSPEC was introduced in 1996. The main difference between the two spectrometers is a larger selection of shaping time parameters available by the DSPECplus.

The DSPECplus unit (dimensions 32.5 cm x 34.8 cm x 14.5 cm) houses the amplifier and ADC components of the spectroscopy system and also supplies the high voltage to the detector. The control of the unit and display of the MCA output is performed using MAESTRO PC based software.

Following the preamplifier stage, the DSPECplus first amplifies, but does not shape, the voltage signal. The signal is then digitized by a continuous-sampling flash ADC. This type of ADC operates by presenting the input pulse simultaneously to a series of threshold comparators in parallel. If the voltage of the comparator is less than that of the

input pulse, a logic signal of 1 is registered, and otherwise the logic signal is registered as 0. The resulting pattern of ones and zeros is converted to a binary number output which represents a digital amplitude of the input pulse.

Following digitization, the input pulse is then shaped using a digital filter. The DSPECplus shapes the pulses as a flat top cusp, or quasi-trapezoid (see figure 2.1). It is possible to change the rise time, flat top width, cusp parameter and tilt of the pulse shape. There are 115 choices for rise time (which also includes the fall time) which range from 0.2 to 23.0 μs in 0.2-μs increments. There are 23 flat top width times ranging from 0.3 to 2.4 μs in 0.1-μs steps. The cusp parameter, which adjusts the curvature or "cuspiness" of the rise and fall times, has 7 possible values ranging from 0.4 to 1 (with the higher values approaching straight lines). The tilt parameter adjusts the "flatness" of the flat top, although this parameter is normally set by using the automated "optimize" function of the DSPECplus, which chooses the best tilt value for the rise time and flat top width selected.

The DSPECplus also offers computer automated pole zero adjustment and baseline restoration. Pole zero restoration is necessary since while the output pulse of the preamplifier has a tail which is quite long, it is not infinitely decaying, and therefore results in a shaped pulse with an undershoot. While this undershoot will eventually return to zero, if another pulse arrives before this time, its full amplitude will not be recorded. Baseline restoration is needed since the shaped pulses return to a non-zero baseline, and this affects the important amplitude information carried by the pulse. The baseline restorer circuit returns the baseline value to zero between each pulse.

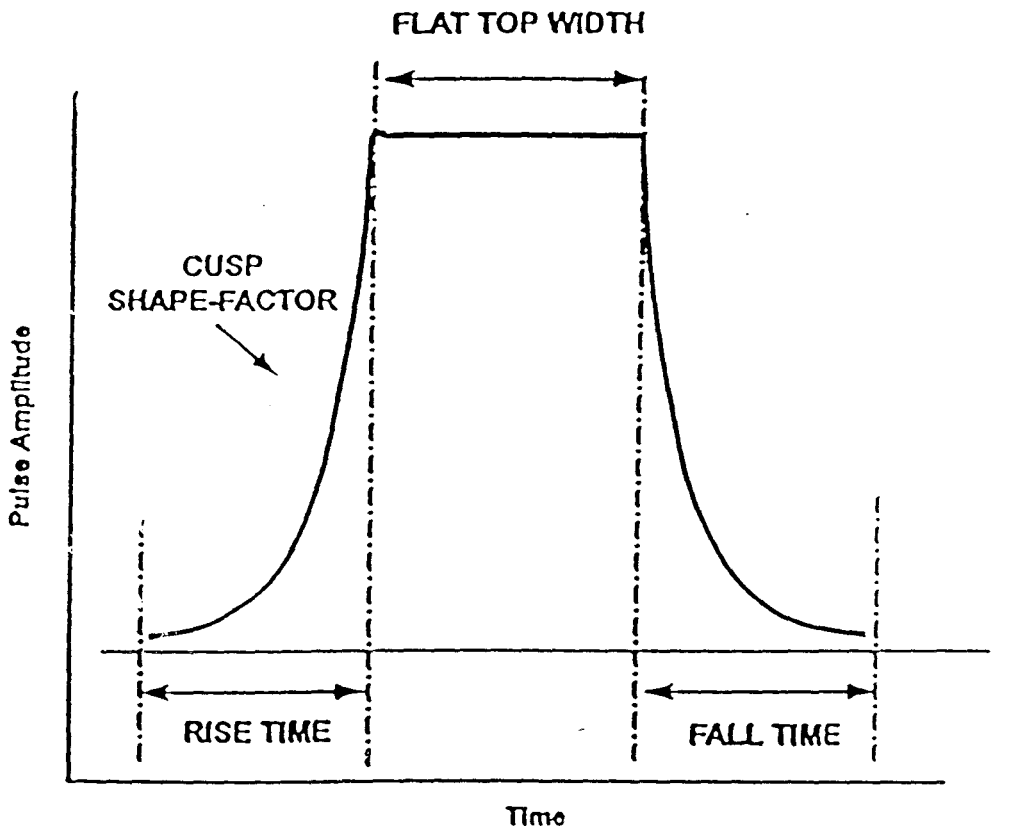

Figure 2.1 DSPECplus Flat Top Cusp Pulse Shape

The amplitude values of the digitally shaped pulses are passed on to the MCA as input, and a pulse height distribution spectrum is created as output.

2.3.2 DSA-2000

The DSA-2000 digital spectrometer was introduced by Canberra in 1997. The unit (dimensions 40.6 cm x 42.5 cm x 8.9 cm) houses the system's amplifier and ADC components, and supplies high voltage to the detector. GENIE-2000 PC based software is used to control the DSA-2000 and display the MCA output.

As with the DSPECplus, the DSA-2000 first amplifies and then digitizes the preamplifier signal using a flash ADC. This digitized signal is then filtered and shaped using digital processing algorithms. The DSA-2000 shapes the pulse as a trapezoid with variable rise times and flat top widths. There are 35 rise time selections ranging from 0.4 to 28 μs. There are 21 possible flat top widths ranging from 0 to 3 μs. The DSA-2000 also offers computer automated pole/zero cancellation and baseline restoration. The MCA stores the amplitude values from the digitally shaped pulses, and displays the information as a pulse height distribution spectrum.

Chapter 3

LEAD INVESTIGATIONS

3.1 Introduction

The measurement of bone lead is important in the area of environmental and occupational health monitoring. The current minimum detection limit (MDL) for the conventional Cd-109 based K XRF system ranges from ~ 6 - 10 μg Pb/g bone mineral. Since the bone lead level for normal subjects ranges from ~ 5 - 25 μg Pb/g bone mineral, a reduction in the current MDL would be beneficial for studies on bone lead metabolism, or on the effects of low-level environmental exposure to lead.

One of the main limitations in the conventional electronics system is the amplifier processing rate. New digital spectrometers, which filter the signals digitally, offer the potential of higher throughput at the amplifier stage without major losses in resolution. These improvements should lead to greater precision in bone lead measurements, and therefore a reduction in the MDL of the system. In 1998, Vo *et al.* compared the DSPEC digital spectrometer with a Standard NIM system in terms of throughput and resolution, using the peaks of Co-57 (122 keV) or Co-60 (1332 keV) sources aimed directly at the detector. At high energies, the DSPEC had better resolution than the NIM system, and for comparable resolutions, the DSPEC had superior throughput performance (Vo *et al.*,

1998). Fleming (1998), carried out a comparison between the DSPEC and a conventional electronics system by making phantom bone lead measurements using a Cd-109 based K XRF system. The results showed a reduction in peak uncertainty of approximately 10 - 15 % by using the DSPEC, which results in an MDL reduction of about 1.0 μg Pb/g bone mineral (Fleming, 1998). In section 3.2 of this chapter, the throughput and resolution performance of a conventional electronics system is compared with that of two new digital spectroscopy systems, the DSPECplus and the DSA-2000, with the improvements in precision related to potential reductions in MDL.

In section 3.3, the throughput, resolution and precision performances of the DSPECplus and DSA-2000 digital spectrometers are compared using two different HpGe detectors. As well, the ability for each detector-spectrometer system to handle high incoming count rate situations is described.

In section 3.4 of this chapter, the application of the DSA-2000 in a bone lead survey is described, and the precision results are compared with those of a previous survey employing conventional electronics. Precision comparisons are also made between bone lead measurements made during these surveys using sources of different strengths.

3.2 Comparison of conventional electronics, DSPECplus, and DSA-2000

3.2.1 Experimental Design

Phantom bone lead measurements were made using a conventional electronics system, a prototype unit of the PerkinElmer DSPECplus digital spectrometer, and the Canberra DSA-2000 digital spectrometer. The K XRF measurements were made using Cd-109 sources in a backscatter geometry. Two different sources were used – one of

strength ~ 0.3 GBq and the other of strength ~ 1.3 GBq. The sources were placed in a tungsten collimator fitted with a 0.5 mm copper shield on the face to filter the Ag K x-rays which are produced in the decay of Cd-109. The source was positioned at the centre of the face of the cylindrical shield which fits over the front end of the HpGe detector to protect the beryllium window.

The measurements were made using three different phantoms: two plaster of Paris (calcium sulphate) phantoms doped with 28 ppm and 0 ppm lead, and a polyester resin phantom containing bone ash but no added lead. The plaster of Paris phantoms were cylinders of diameter 2.5 cm and height 10 cm, and gave a signal representative of bare bone. The resin phantom was a larger cylinder with a diameter of 7.5 cm and height of 10 cm, and gave a signal more representative of an *in vivo* leg measurement. The phantom-source distance was 1.5 cm for the 0.3 GBq source and 3.0 cm for the 1.3 GBq source. The measurements were 30 minutes in length and were repeated 3 times.

The detection system used a Canberra HpGe detector (model GL2020R) (active face 2000 mm^2, thickness 20 mm) operated at - 2500 V and a Canberra charge sensitive preamplifier (model 2001CP) for all measurements.

The conventional system consisted of the following Canberra components: a fast spectroscopy amplifier (model 2024) with a time constant of 1.0 μs, a 450 MHz Wilkinson-type ADC (model 8077), and an S100 multichannel analyzer. This system was previously compared with other conventional electronics systems using Aptec and EG&G Nuclear Instruments components and was found to be superior in terms of resolution and peak error (Cake, 1994).

The DSPECplus digital spectroscopy system and associated MAESTRO software replaced the amplifier, ADC, and MCA components of the conventional system. Shaping parameters were chosen for the system by optimizing the throughput and resolution performance on phantom measurements. Rise times from 1.6 to 2.4 μs, flat top widths from 0.6 to 1.2 μs, and cusp values from 0.6 to 1 were tested (see figure 2.1).

The DSA-2000 spectrometer and GENIE-2000 software replaced the conventional amplifier, ADC, and MCA components. As with the DSPECplus, the DSA-2000 shaping parameters were chosen by optimizing throughput and resolution on phantom measurements. Rise times from 1.0 to 2.4 μs, and flat top widths from 0.6 to 1.2 μs were tested.

The three systems were compared in terms of fractional throughput, coherent peak area and uncertainty, resolution, and potential MDL reduction. The fractional throughput for each measurement was calculated as the ratio of total spectral counts to total incoming counts. The coherent peak area and uncertainty were found using a Marquardt nonlinear least squares fit routine. Resolution was defined as the full width at half maximum (FWHM) of the fitted coherent peak. The potential reduction in MDL was based on the definition of MDL as a peak area equal to twice the uncertainty in the coherent peak, with measurement uncertainty being linearly related to the coherent peak uncertainty. The reductions in coherent peak uncertainty were expressed as a percent reduction compared to the conventional system uncertainty. This percent reduction in peak uncertainty was then related to a potential reduction in MDL.

3.2.2 Results

The results of the rise time, flat top width, and cusp factor trials for the DSPECplus are shown in tables 3.1, 3.2 and 3.3 below. The resolution and peak count values are for the coherent scatter peak. The values are the average of three repeats, and are corrected to real time.

Phantom	Rise Time (μs)	Flat top (μs)	Cusp Factor	Resolution (keV)	Total Spectral Counts (s^{-1})	Peak Net Counts (s^{-1})	Peak Gross Integral (s^{-1})	% Dead Time
28 ppm	1.6	0.9	1.0	0.687	9006	23.91	25.85	7.03
28 ppm	2.0	0.9	1.0	0.680	8955	23.87	25.58	8.10
28 ppm	2.4	0.9	1.0	0.643	8539	22.78	24.50	8.87
0 ppm	1.6	0.9	1.0	0.693	8921	23.70	25.38	6.97
0 ppm	2.0	0.9	1.0	0.667	8786	23.16	24.78	7.95
0 ppm	2.4	0.9	1.0	0.647	8425	22.33	23.88	8.75
Resin	1.6	0.9	1.0	0.667	19447	3.56	5.33	15.98
Resin	2.0	0.9	1.0	0.657	18384	3.41	4.94	17.61
Resin	2.4	0.9	1.0	0.657	17964	3.29	4.82	19.88

Table 3.1 Rise time results for DSPECplus bone lead trials.

Phantom	Rise Time (μs)	Flat top (μs)	Cusp Factor	Resolution (keV)	Total Spectral Counts (s^{-1})	Peak Net Counts (s^{-1})	Peak Gross Integral (s^{-1})	% Dead Time
28 ppm	2.0	0.6	1.0	0.680	8278	22.07	23.70	7.12
28 ppm	2.0	0.9	1.0	0.680	8955	23.87	25.58	8.10
28 ppm	2.0	1.2	1.0	0.670	8262	21.74	23.46	8.00
0 ppm	2.0	0.6	1.0	0.683	8441	22.49	24.08	7.27
0 ppm	2.0	0.9	1.0	0.667	8786	23.16	24.78	7.95
0 ppm	2.0	1.2	1.0	0.677	8404	22.30	23.83	8.14
Resin	2.0	0.6	1.0	0.697	18407	3.49	4.93	16.86
Resin	2.0	0.9	1.0	0.657	18384	3.41	4.94	17.61
Resin	2.0	1.2	1.0	0.687	17419	3.17	4.57	17.81

Table 3.2 Flat top width results for DSPECplus bone lead trials.

Phantom	Rise Time (μs)	Flat top (μs)	Cusp Factor	Resolution (keV)	Total Spectral Counts (s^{-1})	Peak Net Counts (s^{-1})	Peak Gross Integral (s^{-1})	% Dead Time
28 ppm	2.0	1.2	0.6	0.693	9298	24.82	26.83	9.01
28 ppm	2.0	1.2	0.8	0.673	8830	23.59	25.35	8.56
28 ppm	2.0	1.2	1.0	0.670	8262	21.74	23.46	8.00
0 ppm	2.0	1.2	0.6	0.683	9401	25.14	26.88	9.11
0 ppm	2.0	1.2	0.8	0.667	8669	22.98	24.61	8.40
0 ppm	2.0	1.2	1.0	0.677	8404	22.30	23.83	8.14
Resin	2.0	1.2	0.6	0.703	18853	3.63	5.12	19.42
Resin	2.0	1.2	0.8	0.653	17674	3.22	4.65	18.10
Resin	2.0	1.2	1.0	0.687	17419	3.17	4.57	17.81

Table 3.3 Cusp factor results for DSPECplus bone lead trials.

The parameter settings for the DSPECplus tests were chosen as a rise time of 2.0 μs, a flat top width of 0.9 μs, and a cusp factor of 0.8, based on a compromise between high throughput and low resolution values.

The results of the DSA-2000 rise time and flat top width trials are shown in tables 3.4 and 3.5 below. The resolution and peak count values are for the coherent scatter peak. All values are corrected to real time and are the average of three repeats.

Phantom	Rise Time (μs)	Flat top (μs)	Resolution (keV)	Total Spectral Counts (s^{-1})	Peak Net Counts (s^{-1})	Peak Gross Integral (s^{-1})	% Dead Time
0 ppm	1.0	0.9	0.773	10262	26.91	28.81	4.43
0 ppm	1.6	0.9	0.705	9934	26.15	27.95	6.48
0 ppm	2.0	0.9	0.658	9397	24.92	26.66	7.12
0 ppm	2.4	0.9	0.640	8943	23.96	25.59	7.83
Resin	1.0	0.9	0.801	26755	4.88	6.91	11.70
Resin	1.6	0.9	0.686	24035	4.48	6.29	15.66
Resin	2.0	0.9	0.639	21575	4.02	5.63	16.63
Resin	2.4	0.9	0.637	18122	3.31	4.78	16.37

Table 3.4 Rise time results for DSA-2000 bone lead trials.

Phantom	Rise Time (μs)	Flat top (μs)	Resolution (keV)	Total Spectral Counts (s^{-1})	Peak Net Counts (s^{-1})	Peak Gross Integral (s^{-1})	% Dead Time
0 ppm	1.6	0.6	0.721	9577	25.20	26.93	5.48
0 ppm	1.6	0.9	0.705	9934	26.15	27.95	6.48
0 ppm	1.6	1.2	0.683	9174	24.24	25.88	7.06
Resin	1.6	0.6	0.709	24140	4.44	6.36	14.43
Resin	1.6	0.9	0.686	24035	4.48	6.29	15.66
Resin	1.6	1.2	0.651	22472	4.22	5.79	17.33
0 ppm	2.4	0.9	0.640	8943	23.96	25.59	7.83
0 ppm	2.4	1.2	0.643	10147	27.23	29.09	9.63
Resin	2.4	0.9	0.637	18122	3.31	4.78	16.37
Resin	2.4	1.2	0.627	20479	3.83	5.50	20.25

Table 3.5 Flat top width results for DSA-2000 bone lead trials.

The parameter settings for the DSA-2000 tests were chosen as a rise time of 2.4 μs and a flat top width of 1.2 μs based on a compromise between high throughput and low resolution.

Figure 3.1 shows the fractional throughput for each system at differing incoming count rates. The higher incoming count rates correspond to the 1.3 GBq source trials using the resin phantom, while the lower incoming count rates are from the 0.3 GBq source trials with the plaster of Paris phantoms. For all of the systems, the fractional throughput is greater at lower incoming count rates. The two digital systems show very similar fractional throughput results, and at all incoming count rates they show superior performance to the conventional system. The difference between the digital and conventional systems was much more significant at the higher incoming count rates. At very low incoming count rates (~ 10 000 cps), the digital systems had fractional throughputs of ~ 0.9 while the conventional system value was ~ 0.85. However, at an incoming count rate of ~ 85 000 cps, the fractional throughput for the digital systems was ~ 0.5, while it was only ~ 0.3 for the conventional system. The digital spectrometers

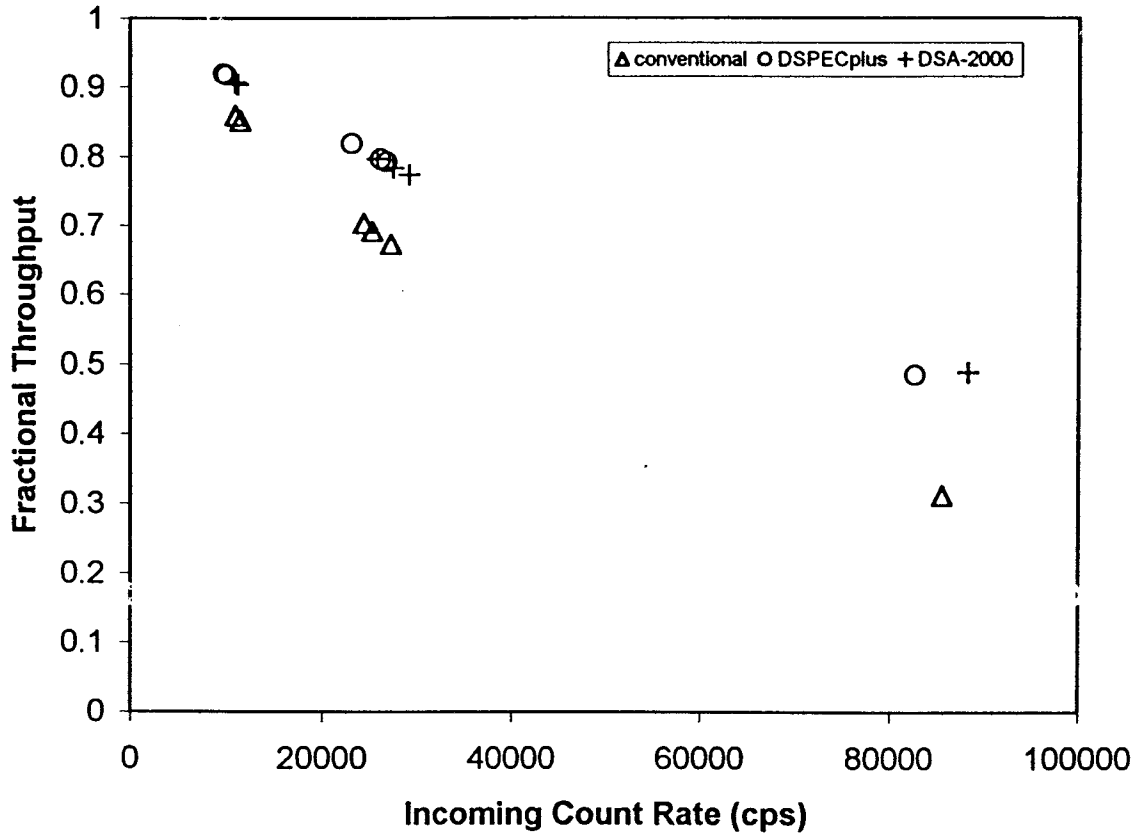

Figure 3.1 Fractional Throughput at Differing Incoming Count Rates

show superior ability to process pulses in situations where the system is "pushed" with a high incoming count rate.

The coherent peak area, peak uncertainty, and resolution results for the phantom tests are shown in Table 3.6 below. The values are the average of three repeats and are corrected to real time.

		0.3 GBq Source			1.3 GBq Source		
System	Phantom	Peak Area (counts)	Peak Uncertainty (%)	Resolution (eV)	Peak Area (counts)	Peak Uncertainty (%)	Resolution (eV)
Conventional	28 ppm	47907 +/- 292	0.61	685.2 +/- 2.9	81961 +/- 422	0.51	703.3 +/- 2.6
	0 ppm	45767 +/- 283	0.62	683.1 +/- 2.9	78299 +/- 407	0.52	701.5 +/- 2.6
	Resin	6008 +/- 112	1.86	676.6 +/- 9.7	9952 +/- 193	1.94	736.7 +/- 11.5
DSPECplus (prototype unit)	28 ppm	42880 +/- 287	0.67	676.9 +/- 3.1	94727 +/- 446	0.47	688.9 +/- 2.2
	0 ppm	44132 +/- 289	0.65	680.4 +/- 3.0	93399 +/- 440	0.47	690.9 +/- 2.2
	Resin	6240 +/- 128	2.05	672.4 +/- 10.4	14657 +/- 254	1.73	761.2 +/- 10.2
DSA-2000	28 ppm	47910 +/- 292	0.61	630.4 +/- 2.5	101492 +/- 448	0.44	633.3 +/- 1.9
	0 ppm	49298 +/- 293	0.59	631.6 +/- 2.5	97126 +/- 435	0.45	633.5 +/- 1.9
	Resin	6880 +/- 125	1.82	623.6 +/- 8.3	16412 +/- 231	1.41	637.4 +/- 6.7

Table 3.6 Coherent peak area counts, peak uncertainty, and resolution for bone lead trials.

For all of the systems, the lowest number of coherent peak counts, and the highest peak uncertainty, was found with the resin phantom. Compared with the plaster of Paris phantoms, the resin phantom has less mineral content to contribute to coherent scattering, but more components in the polyester resin to contribute to Compton scattering, which leads to the increased uncertainty. Because of these factors, the resin results are similar to the results which would be expected for an *in vivo* tibia measurement.

For all three systems, the trials with the 1.3 GBq source resulted in significantly higher peak counts and slightly worsened resolution compared to the 0.3 GBq trials. The digital systems showed an improvement in peak uncertainty for all phantoms with the 1.3 GBq source, while the conventional system showed a slight improvement for the plaster of Paris phantoms, and a slight worsening in peak uncertainty for the resin phantom using the hotter source.

The greatest differences between the three systems were seen for the 1.3 GBq source and resin phantom trials. In both of these instances, the systems were required to handle higher incoming count rates, and the digital spectroscopy systems both performed better than the conventional system under these conditions. For the 1.3 GBq source and resin phantom measurements, the greatest throughput (indicated by coherent peak counts) and lowest peak uncertainty was achieved by the DSA-2000 (16421 +/- 1.41 %), followed by the DSPECplus (prototype unit) (14657 +/- 1.73 %), and then the conventional system (9952 +/- 1.94 %). The best resolution was achieved by the DSA-2000 (637.4 +/- 6.7 eV), followed by the conventional system (736.7 +/- 11.5 eV), and then the DSPECplus (prototype unit) (761.2 +/- 10.2 eV).

A comparison of the best peak uncertainties seen for the DSA-2000 and the conventional system, for the resin phantom trials, shows an improvement of 24.2 % by the DSA-2000. To relate this improvement in precision to a potential MDL decrease, the current uncertainty of ~ 3 – 5 μg Pb/g bone mineral found with conventional systems is used as a reference value. Since this uncertainty value equates to an MDL of 6 – 10 μg Pb/g bone mineral, the 24.2 % improvement in uncertainty found by using the DSA-2000

would correspond to a potential MDL reduction of approximately 1.5 – 2.5 μg Pb/g bone mineral. For the DSPECplus (prototype unit), an improvement in peak uncertainty of 7.0 % compared to the conventional system was seen. The resulting potential MDL reduction found by using this prototype DSPECplus unit would be approximately 0.4 – 0.7 μg Pb/g bone mineral.

The inferior DSPECplus values were likely due to problems with the pole zero adjustment on the prototype unit. According to PerkinElmer, several DSPECplus units manufactured at the same time as the one used for testing had automatic pole zero functions which would improperly adjust the pole zero at high incoming count rates. As this was the case for the 1.3 GBq source and resin phantom trials, a repeat of these trials with a new commercial DSPECplus unit was done. At the time of the repeat trials, the source had decayed to a strength of ~ 0.8 GBq. The same sample-source distance, spectrometer settings, and measuring times were used as for the earlier trials. The measurement was also repeated with the DSA-2000 for comparison purposes. The results of the two repeated trials are shown in Table 3.7 below.

System	Phantom	Peak Area (counts)	Peak Uncertainty (%)	Resolution (eV)
DSPECplus	Resin	11298 +/- 204	1.81	556.7 +/- 6.4
DSA-2000	Resin	12148 +/- 208	1.71	548.1 +/- 5.9

Table 3.7 Repeated DSPECplus and DSA-2000 resin phantom measurements.

It can be seen from the results of the repeated measurements that the difference between the two digital spectrometers is very small. It is very probable that the pole zero function on the prototype unit was the reason for the poorer DSPECplus performance in the earlier tests. With the new commercial DSPECplus unit, improvements in peak uncertainty and

resulting reductions in MDL would likely be in the same range as the 24.2 % and 1.5 – 2.5 μg Pb/g bone mineral which were found with the DSA-2000.

The superior pulse processing abilities and reductions in peak uncertainty achieved by using the digital spectroscopy systems are a significant step in improving current bone lead measurement systems. The reductions in MDL found by using the DSA-2000 and DSPECplus allow the current MDL of 6 – 10 μg Pb/g bone mineral to be reduced to a level below, or at the very low end of, the normal bone lead level range of 5 – 25 μg Pb/g bone mineral. This improved measurement precision and reduction in MDL would allow for more reliable monitoring of the bone lead levels of occupationally exposed workers, as well as the measurement of bone lead levels for studies on lead metabolism or the effects of low-level environmental lead exposure.

3.3 New Detector

3.3.1 Experimental Design

Phantom bone lead measurements were made using two different digital spectrometers (the PerkinElmer DSPECplus and the Canberra DSA-2000), and two different HpGe detectors (the PerkinElmer LOAX model 51700/20-S and the Canberra model GL2020R). A Cd-109 source of strength ~ 0.8 GBq was placed in a backscatter geometry as described in section 3.2.1 to make the K XRF measurements.

The phantom measurements were made using a cylindrical polyester resin phantom (diameter 2.5 cm, height 10 cm) containing bone ash but no added lead. The measurements were 30 minutes in length and were repeated 3 times.

The Canberra HpGe detector and preamplifier system was the same system which was used for the investigations described in section 3.2.1. The new detector tested here was a PerkinElmer LOAX HpGe detector with a crystal diameter of 52.0 mm, length 20.0 mm, and operating voltage of – 3400 V. A PerkinElmer charge sensitive preamplifier (model 257N) was integral with this detector. The DSA-2000 spectrometer and associated software components were the same as those used for the previous investigations. The DSPECplus spectrometer used in these investigations was a commercial unit, a different unit from the prototype unit that was used for the previous experiments.

Before the phantom measurements were made, the optimal rise times, flat top widths, and, for the DSPECplus, cusp values were determined for each spectrometer-detector system. For this determination a "merit value" method was used. This method involved pointing the Cd-109 source directly at the detector with the MCA software set to run for a fixed preset of 1 000 000 gross integral counts in the 88 keV peak. The "merit value" was defined as the product of the FWHM of the 88 keV peak and the real time for the measurement, with the lowest merit value being the most optimal.

Initially, the best distances at which to perform the shaping parameter optimization tests were determined. This was done by performing the merit value tests with the Cd-109 source at differing distances from the detector for each spectrometer-detector combination, with the best distance being that with the lowest merit value. These initial distance measurements were all done with a rise time of 2.0 μs, flat top width of 0.9 μs, and, for the DSPECplus, a cusp value of 1.0. They were later repeated at the optimal

settings determined for each system to compare how the systems handled differing incoming count rates in terms of peak resolution and total spectral throughput.

Once the best distance was determined, different rise times, flat top widths, and cusp values were tested for each system, and the settings with the lowest merit values were chosen as optimal.

For the LOAX - DSPECplus system, settings of 2.0 μs rise time, 0.6 μs flat top width, and 1.0 cusp shape factor were chosen as the optimal settings. By using the resin phantom and merit value method, it was determined that the best sample-source distance for the phantom measurements would be 0.5 cm.

For the LOAX – DSA-2000 system, the optimal settings were found to be a rise time of 1.6 μs and flat top width of 0.6 μs. Again, a sample-source distance of 0.5 cm was used for the resin phantom measurements.

For the Canberra HpGe – DSPECplus system, the optimal settings were found to be a 2.0 μs rise time, 0.9 μs flat top width, and 1.0 cusp shape factor. For the resin phantom measurements with this spectrometer-detector combination, the best sample-source distance was found to be 1.5 cm, with distances any closer resulting in distorted spectra.

For the Canberra HpGe – DSA-2000 system, the optimal settings were found to be a rise time of 1.6 μs and flat top width of 0.6 μs. Again, a sample-source distance of 1.5 cm was used for the resin phantom measurements.

In order to compare with the measurements made using the Canberra HpGe detector better, the measurements made using the LOAX detector were repeated using a sample-source distance of 1.5 cm. As well, the measurements made with the DSPECplus

spectrometer were repeated using settings of 1.6 μs rise time, 0.6 μs flat top width, and 1.0 cusp shape factor, in order to compare with the DSA-2000 measurements better.

The results from the phantom measurements using the four different spectrometer-detector systems were compared in terms of peak area, uncertainty and resolution of the fitted coherent peak. The calculation of these quantities was the same as was described in section 3.2.1 for the previous lead investigations.

3.3.2 Results

The results from the measurements made by pointing the Cd-109 source at the detector at different distances are shown in figures 3.2 and figure 3.3. Each figure shows both the total spectral throughput and the resolution (FWHM) of the 88 keV peak as a function of the incoming count rate. These results are from the measurements which were made using the optimal shaping parameters for each system.

Figure 3.2 shows the results for the LOAX detector and the DSPECplus and DSA-2000 spectrometers. For both detector-spectrometer combinations, a maximum throughput is reached which then gradually decreases as the incoming count rate increases. At the highest incoming count rate for both systems (very high rates of ~ 500 000 – 600 000 cps), the source is almost touching the detector face, yet there is no spectral distortion and there is little loss in resolution of the 88 keV peak. The best throughput for the DSPECplus was ~ 47 000 cps at an incoming count rate of ~ 125 000 cps. The DSA-2000, however, had a much greater maximum throughput of ~ 76 000 cps which occurred at an incoming count rate of ~ 240 000 cps. The actual source-detector

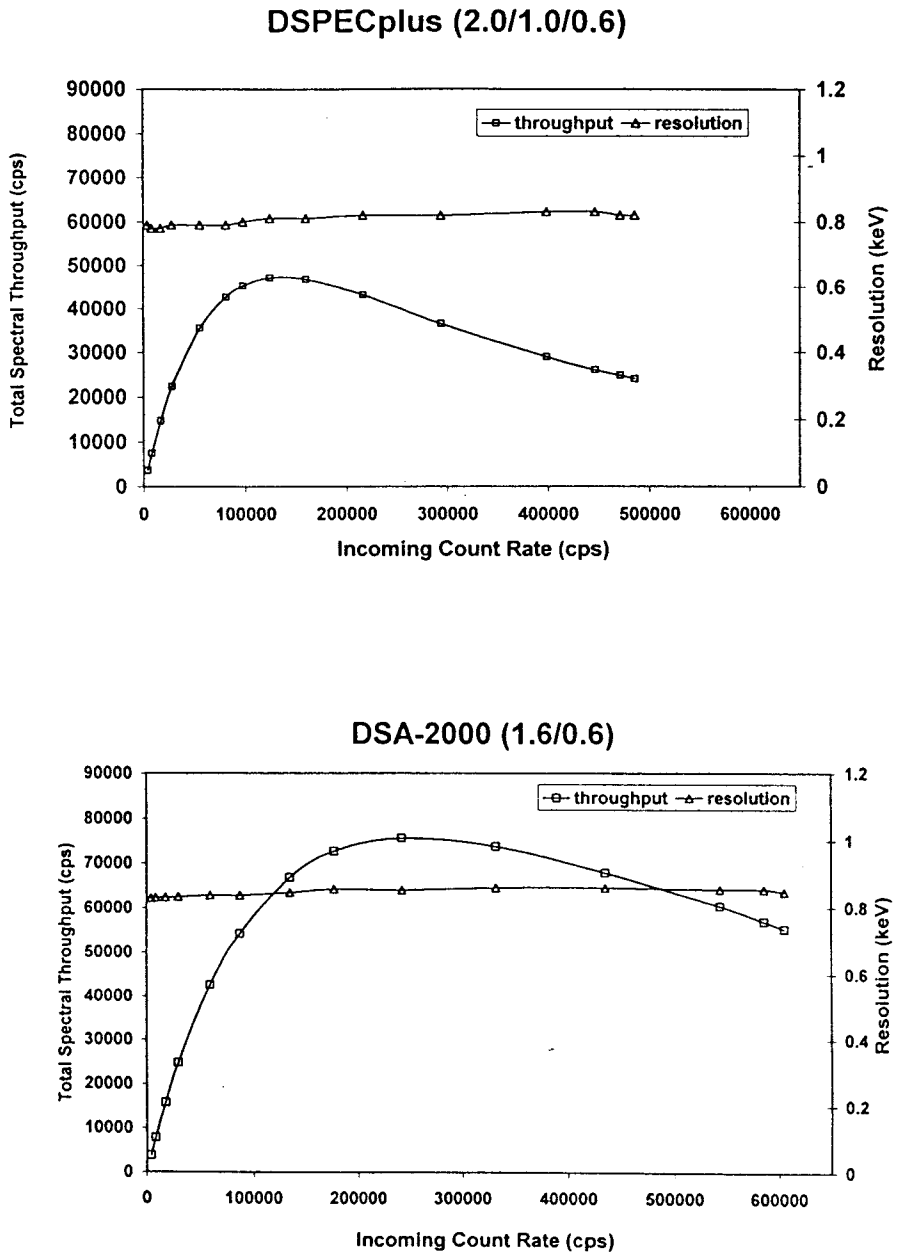

Figure 3.2 Total Spectral Throughput and Resolution at Differing Incoming Count Rates: LOAX Detector

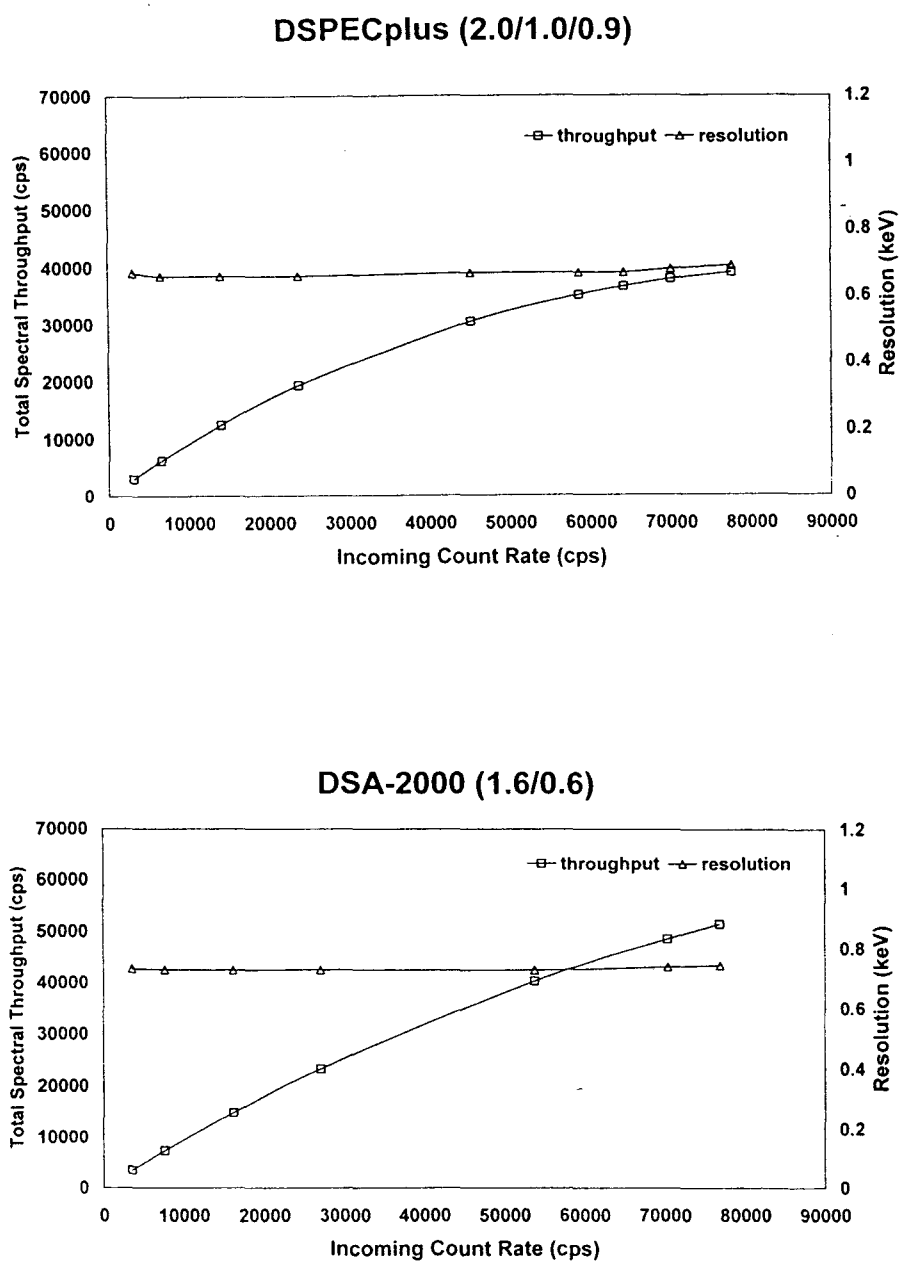

Figure 3.3 Total Spectral Throughput and Resolution at Differing Incoming Count Rates: Canberra HpGe Detector

distances for these maxima were ~ 6.0 cm and ~ 4.0 cm for the DSPECplus and DSA-2000 respectively.

Figure 3.3 shows the results for the Canberra HpGe detector and the DSPECplus and DSA-2000 spectrometers. Here, a maximum throughput is reached at much lower incoming count rates, after which the spectra become distorted. This difference is possibly due to differences in the preamplifiers of the two detector systems. For the DSPECplus, this maximum throughput was ~ 39 000 cps at an incoming count rate of ~ 78 000 cps (a distance of ~ 7.0 cm from the detector). While the throughput from this combination is not as great as that for the LOAX – DSPECplus combination (~ 47 000 cps), the resolution is better (~ 0.67 keV compared with ~ 0.81 keV for the LOAX). For the Canberra HpGe – DSA-2000 combination, the maximum throughput was ~ 51 000 cps at an incoming count rate of ~ 77 000 cps (at a distance of ~ 8.0 cm). This throughput is not as great as the maximum found with the LOAX – DSA-2000 (~ 76 000 cps), however the resolution is better (~ 0.73 keV compared with ~ 0.85 keV for the LOAX).

The distance test results for the LOAX detector showed greater throughput yet worsened resolution compared to the Canberra HpGe detector for both the DSPECplus and DSA-2000. The results for the DSA-2000 tests showed greater throughput than for the DSPECplus tests. While the resolution results for the DSA-2000 were worse than those for the DSPECplus, these values cannot necessarily be directly compared as they were taken from the software display from each system. In order to compare between the four combinations better, the merit values can be used. The best merit value for each

system occurred at the maximum throughput value and were as follows: LOAX – DSPECplus: 23.3, LOAX – DSA-2000: 15.7, Canberra HpGe – DSPECplus: 24.1, Canberra HpGe – DSA-2000: 19.7. This comparison shows that for the merit value test and distance measurements, the LOAX performs better than the Canberra HpGe, and that the DSA-2000 performs better than the DSPECplus.

The coherent peak area, peak uncertainty and resolution results for the resin phantom measurements are in table 3.8. The values are the average of three repeats.

Detector	Spectrometer	Settings (rise time/ cusp/ flat top)	Distance (cm)	Peak Area (counts)	Peak Uncertainty (%)	Resolution (eV)
LOAX	DSPECplus	2.0/1.0/0.6	0.5	8702 +/- 198	2.28	732.8 +/- 12.0
LOAX	DSA-2000	1.6/ - /0.6	0.5	9567 +/- 205	2.15	705.1 +/- 10.5
LOAX	DSPECplus	2.0/1.0/0.6	1.5	16202 +/- 280	1.73	730.2 +/- 9.4
LOAX	DSA-2000	1.6/ - /0.6	1.5	21316 +/- 341	1.60	725.7 +/-8.7
Canberra HpGe	DSPECplus	2.0/1.0/0.9	1.5	14102 +/- 235	1.66	568.6 +/- 6.1
Canberra HpGe	DSA-2000	1.6/ - /0.6	1.5	22938 +/- 310	1.35	612.3 +/- 5.5
LOAX	DSPECplus	1.6/1.0/0.6	1.5	18370 +/- 359	1.95	879.1 +/- 14.4
Canberra HpGe	DSPECplus	1.6/1.0/0.6	1.5	16148 +/- 283	1.75	658.9 +/- 7.8

Table 3.8 Coherent peak area counts, peak uncertainty, and resolution for resin phantom measurements.

While the original LOAX phantom tests were performed at a sample-source distance of 0.5 cm (as this was what was indicated as the best distance using merit value tests), the 1.5 cm measurements show superior results. For both the DSPECplus and DSA-2000, the peak area values are greater and the peak uncertainties are lower, with resolution

staying fairly constant, for the 1.5 cm tests. This would indicate that at the very close distance of 0.5 cm, the resin phantom tests cannot be compared to the situation of aiming a source directly at the detector, and for that reason the merit value method failed. It is possible that with the resin phantom there is self shielding at this close distance so that the radiation emitted from the phantom is not able to reach the detector.

Comparing the DSPECplus and DSA-2000 values for the LOAX, optimal setting, 1.5 cm tests, it can be seen that the DSA-2000 shows better results. While the resolutions are similar, the DSA-2000 peak throughput is greater (21 316 vs. 16 202 counts) and peak uncertainty is less (1.60 vs. 1.73 %) than the DSPECplus.

Comparing the DSPECplus and DSA-2000 values for the Canberra HpGe optimal setting trials, it can be seen that again the DSA-2000 has better results. Here, peak area is greater (22 938 vs. 14 102 counts) and peak uncertainty is less (1.35 vs. 1.66 %) for the DSA-2000. The resolution of the DSPECplus trials, however, is lower than that of the DSA-2000 trials (568.6 vs. 612.3 eV).

Measurements done using the LOAX and Canberra HpGe detectors with the DSPECplus using settings of 1.6 μs rise time, 0.6 μs flat top width, and 1.0 cusp factor showed inferior results when compared to the measurements made using the optimal parameter settings for these systems. While the throughput was increased, the resolution and peak uncertainty values both worsened.

Comparing the results from the LOAX and Canberra HpGe detectors, superior performance is seen from the Canberra detector in terms of peak area, uncertainty and resolution for both the DSPECplus and DSA-2000 (with the exception of the DSPECplus

peak area results which are greater for the LOAX than for the Canberra HpGe). The best overall results are seen for the Canberra HpGe – DSA-2000 combination with a peak area of 22 938 counts, peak uncertainty of 1.35 %, and resolution of 612.3 eV. The second best results were from the LOAX – DSA-2000 combination, followed by the Canberra HpGe – DSPECplus, and then the LOAX – DSPECplus.

While the earlier distance trial results indicated that the LOAX should perform better than the Canberra HpGe detector, these results were based on the merit value test applied to a source pointed directly at the detector. For the resin phantom tests, the Canberra HpGe detector clearly showed better precision and throughput results.

The merit value optimization tests for the Canberra HpGe – DSPECplus combination resulted in shaping parameters very similar to those chosen for the earlier tests described in section 3.2.2 (2.0/1.0/0.9 versus 2.0/0.8/0.9 previously chosen). For the more recent tests, the peak uncertainty of 1.66 % found translates to a precision improvement of 10.8 % compared with conventional electronics. While this improvement is better than the 7.0 % improvement previously seen with the prototype DSPECplus unit, it is not as good as the predicted ~ 24.2 % improvement expected if a commercial DSPECplus unit had been tested with the 1.3 GBq source and resin phantom.

The results from the Canberra HpGe – DSA-2000 tests show that there is a slight improvement in precision compared to that found in the previous tests described in section 3.2.2. In the earlier trials, the shaping parameter values were 2.4/1.2, and were chosen by finding the best compromise between throughput and resolution without using any specific formula. In the more recent trials, the parameters were 1.6/0.6 and were

chosen using the merit value test. It appears that the previous method of choosing parameters for the DSA-2000 weighted the effect of resolution too heavily at the cost of throughput, which resulted in a non-optimal choice of settings. The results of the more recent tests were a precision of 1.35 %, and a precision improvement of 27.4 % which are slightly better than the previous values of 1.41 % and 24.2 %. It is unlikely that these results could be improved by using a hotter source since the detector was already operating at its maximum throughput capacity for these most recent trials.

The results of the digital spectrometer–detector tests show that the best combination for the bone lead measurement application is the Canberra HpGe – DSA-2000. This measurement system, with parameter settings chosen using the merit value method described above, showed the best precision improvements compared with the conventional electronics system.

3.4 Brunswick Mining and Smelting Bone Lead Survey

3.4.1 Introduction

In 1994 and 1999, McMaster University participated in bone lead surveys at the Brunswick Mining and Smelting lead smelter in Belledune, New Brunswick. Occupational monitoring of the employees' lead exposure is primarily done by testing blood lead levels, which are most useful as an indicator of recent lead exposure. The two bone lead surveys have been useful in terms of providing an indication of long term lead exposure and retention, and for studying lead metabolism over time. In 1994, conventional electronics systems were used to measure both the tibia and calcaneus bone lead levels, while in 1999, a conventional system was used to measure the tibia, and the

DSA-2000 digital system was used to measure the calcaneus. With *in vivo* XRF measurements, it is important to have the best precision and lowest MDL possible in order to improve the reliability and range of the measurements. A comparison of the precision values found in the two bone lead surveys is described below.

3.4.2 Experimental Method

In the 1994 bone lead survey, K XRF measurements of the tibia and calcaneus were made using conventional electronics systems consisting of components as described for the McMaster University lead detection system in section 2.2. Cd-109 sources of activity 0.9 GBq were used in a backscatter geometry. The source-sample distances were approximately 2.0 cm, and the measurements were 30 minutes (live time) in length (Fleming *et al.*, 1997). A set of plaster of Paris bone phantoms with known amounts of lead (ranging from 0 to 200 ppm) was used to generate calibration lines. The lead concentrations in the tibia and calcaneus were determined by using the Marquardt-based fitting routine described in section 1.3.2.

In the 1999 bone lead survey, K XRF measurements of the tibia were made with the same conventional electronics system as was used in 1994. The calcaneus measurements were made using the same model of detector and preamplifier, but the amplifier, ADC, and MCA components were replaced with a DSA-2000 unit and its associated GENIE-2000 software. The DSA-2000 shaping parameters were set at a 2.0 μs rise time and a 0.9 μs flat top width. Cd-109 sources in a backscatter geometry were again used to make 30 minute live time measurements. A set of calibration phantoms was used to generate

calibration lines and the same Marquardt-based fitting routine was used to determine the lead concentrations for the tibia and calcaneus.

For the 1999 survey, several different source strengths were used. During the initial part of the survey, sources of 0.3 GBq were used for both the tibia and calcaneus measurements. For these measurements, the source-sample distance was approximately 2 cm. New sources of higher activity (1.3 GBq) were used for the next part of the survey, with a source-sample distance of about 3 cm. For the calcaneus measurements, this 1.3 GBq source was used for the remainder of the survey. However, for the tibia measurements, the 1.3 GBq source was replaced by the original two 0.3 GBq sources for the rest of the survey, with a source-sample distance of about 2.5 cm. This replacement was made since the conventional system's performance had declined with the hotter 1.3 GBq source.

3.4.3 Results

The frequency distributions for the precision values are shown in figure 3.4 for the tibia measurements, and in figure 3.5 for the calcaneus measurements. The 0.3 GBq sources are referred to as "old", and the 1.3 GBq sources are referred to as "new". Measurements referred to as "repeat" measurements only include the 1999 measurements for those individuals who were also measured in the 1994 survey.

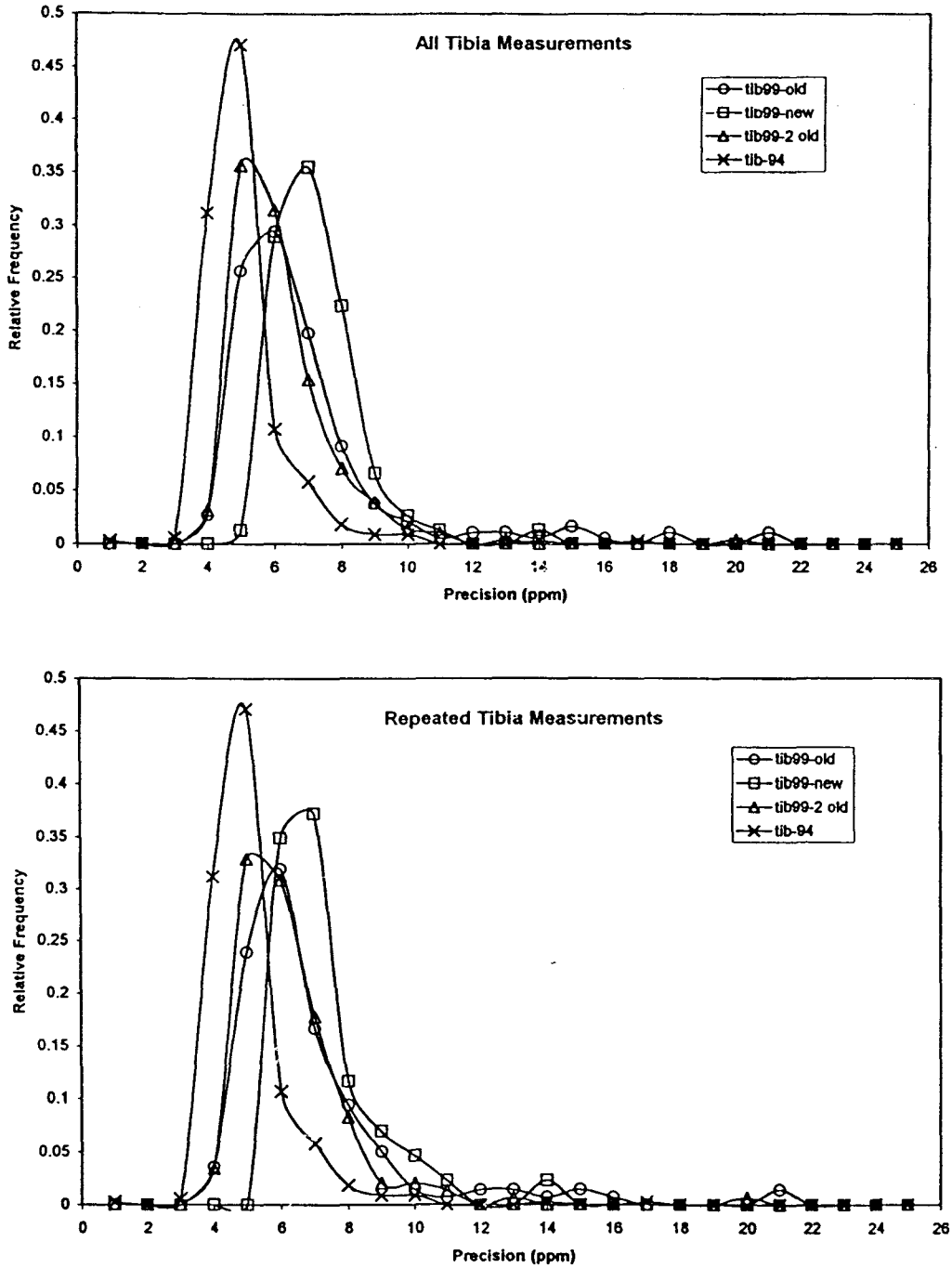

Figure 3.4 Precision Distributions of Tibia Measurements for 1994 and 1999 Bone Lead Surveys

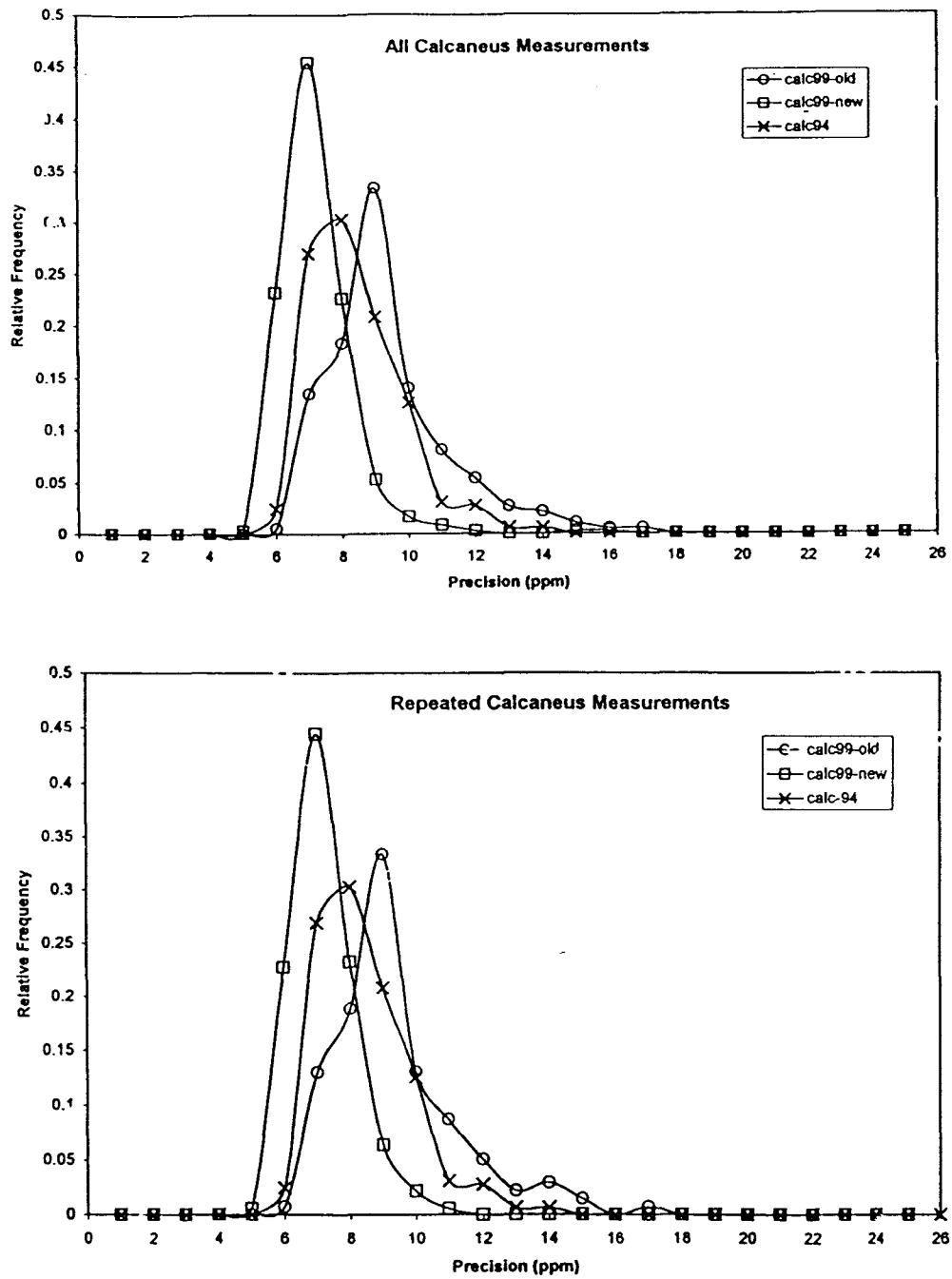

Figure 3.5 Precision Distributions of Calcaneus Measurements for 1994 and 1999 Bone Lead Surveys

The mean, standard deviation, and median precision results for the bone lead surveys are shown in Table 3.9 below.

Survey Group	Mean	Standard Deviation	Median	Minimum	Maximum	n
All Tibia '99 Old Source	6.46 +/- 0.20	2.80	5.70	3.89	20.62	187
All Tibia '99 New Source	6.77 +/- 0.15	1.34	6.52	4.97	13.20	76
All Tibia '99 2 Old Sources	5.73 +/- 0.12	1.98	5.28	3.50	25.76	286
Repeat Tibia '99 Old Source	6.47 +/- 0.24	2.77	5.64	3.92	20.62	138
Repeat Tibia '99 New Source	6.82 +/- 0.25	1.62	6.50	5.12	13.20	43
Repeat Tibia '99 2 Old Sources	5.80 +/- 0.15	1.85	5.43	3.64	19.33	146
Tibia '94	4.61 +/- 0.08	1.35	4.29	0.92	16.08	327
All Calcaneus '99 Old Source	8.87 +/- 0.14	1.86	8.66	5.99	16.02	186
All Calcaneus '99 New Source	6.75 +/- 0.06	1.15	6.59	4.94	15.60	363
Repeat Calcaneus '99 Old Source	8.88 +/- 0.16	1.88	8.65	5.99	16.02	138
Repeat Calcaneus '99 New Source	6.71 +/- 0.07	0.93	6.54	4.94	10.07	189
Calcaneus '94	7.96 +/- 0.08	1.39	7.82	5.50	13.04	327

Table 3.9 Precision comparison between 1994 and 1999 bone lead surveys. (precision values are in μg Pb/g bone mineral)

As can be seen from the frequency distributions and average precision values, the tibia precision found in the 1994 survey was superior to that found in the 1999 survey, for all of the 1999 source configurations. The best median precision found in 1999 for the repeated group was for the "2 old source" configuration (5.43 μg Pb/g bone mineral), which is significantly larger than the median precision found for the same group of

individuals in 1994 (4.29 μg Pb/g bone mineral). Since both detection systems used the same components, this great a difference would not be expected. The poorer results were possibly due to a decrease in the throughput performance of the detector used during the 1999 survey. Before the survey, the maximum throughput of the detector was ~ 40 000 cps. After the survey, the maximum throughput was found to be only ~ 28 000 cps. Several months later, the detector was completely warmed up and then cooled down, after which the maximum throughput was again ~ 40 000 cps. If the detector was partially warmed up during its transport to the survey site, some residual gases may have been absorbed by the detector surfaces and become frozen there during the cooling down process. The performance of the detector was able to be later restored because the complete warm up and cool down process allows the molecular sieve of the detector to pump the system clean of impurities (Canberra, 1991). As well, the precision variation between the two surveys could also be partially due to the differences in source strengths and sample-source distances which were used.

Within the 1999 tibia survey results, the best precision was found with the "2 old source" configuration. The median precision for this group was 5.28 μg Pb/g bone mineral, compared with 6.52 μg Pb/g bone mineral for the "new source" configuration and 5.70 μg Pb/g bone mineral for the "old source" configuration. The switch to this intermediate source strength configuration from the hotter, 1.3 GBq source was a beneficial decision in terms of improving the tibia precision results found using the conventional electronics system. The difference in precision seen here between the "old" and the "new" source (14.4 %) was greater than that seen for the phantom measurements

described in the section 3.2. The percent difference between the conventional system resin phantom results for the 0.3 GBq and 1.3 GBq sources was only 4.3 %. The difference between the *in vivo* and phantom results could be due to the difference in sample-source distance for the 0.3 GBq measurements (2.0 cm for the survey versus 1.5 cm for the phantom tests), or because of differences between the resin leg phantom and the true subject shin.

It can be seen from the frequency distributions and average precision results that the best precision for the calcaneus measurement was obtained using the DSA-2000 and "new" source. For this configuration, the median precision was 6.54 μg Pb/g bone mineral for the repeated values, while for the "old" source/DSA-2000 configuration it was 8.65 μg Pb/g bone mineral. The median precision for the 1994 measurements made on the same individuals using conventional electronics was 7.82 μg Pb/g bone mineral. It is clear that the combination of digital electronics and a high incoming count rate allow for superior precision performance compared to that seen using conventional electronics, or a low incoming count rate. The use of the DSA-2000 and "new" source allowed for a 16.4 % improvement in measurement precision compared to the conventional system used in 1994. This improvement is not as great as the 24.2 % improvement in precision found in the phantom studies described in section 3.2 comparing the DSA-2000 and conventional system performance. However, the source strengths and sample-source distances were not the same for the two conventional systems being compared. The phantom study DSA-2000 system was compared to a conventional system with a 0.3 GBq source and 1.5 cm distance, while the survey DSA-2000 system was compared to a

conventional system with a 0.9 GBq source and 2.0 cm distance. The lesser degree of precision improvement seen with the survey results could also be due to other differences in the conventional systems used in the two studies, or because of differences between the resin leg phantom and the true subject heel.

The effect of source strength on precision is also seen when comparing all of the 1999 calcaneus measurements. Here the "new" source median precision is 6.59 μg Pb/g bone mineral, while the "old" source median precision is 8.66 μg Pb/g bone mineral, where both measurements were done using the DSA-2000. The percent difference in precision seen here (23.9 %) is comparable to that seen with the phantom tests described in section 3.2. In the DSA-2000 and resin phantom experiments, the percent difference between the precisions found for the 0.3 GBq and 1.3 GBq sources was 22.5 %, only slightly different from that found for the *in vivo* measurements.

The results of these surveys indicate that the use of digital spectroscopy, in combination with a strong excitation source, results in improved precision performance for the *in vivo* XRF measurement of bone lead. This improvement is important in increasing the reliability of the measurements, as well as reducing the MDL of the system. Occupational monitoring of those with low amounts of lead exposure, and better ability to detect changes in bone lead levels over time, are other improvements that are possible with this *in vivo* measurement application of digital spectroscopy.

Chapter 4

MERCURY INVESTIGATIONS

4.1 Introduction

The *in vivo* XRF measurement of kidney mercury would be a valuable tool in the occupational monitoring of those exposed to mercury in the workplace. Börjesson *et al.* (1995) measured the kidney mercury levels of 20 occupationally exposed workers and 12 referents using polarized x-ray fluorescence. The mean kidney mercury level in the exposed group was 24 μg/g while the mean level in the unexposed group was 1 μg/g. The mean MDL for the system was 26 μg/g, with 9 of the exposed workers exceeding this limit, and none of the referents exceeding it. Before this measurement is considered a reliable occupational monitoring technique, improvements in the MDL of the system need to be made. In 1999, O'Meara showed that increasing the x-ray tube voltage reduced the MDL of the system significantly (for example, increasing the voltage from 175 kVp to 250 kVp reduced the MDL from 39 +/- 4 μg/g to 26 +/- 1 μg/g). This chapter will describe the improvement in MDL gained by utilizing the DSA-2000 digital spectrometer to use digital filtration for the pulses in place of a conventional electronics processing system.

4.2 Comparison of conventional electronics and DSA-2000

4.2.1 Experimental Design

The measurements were performed using a polarized x-ray fluorescence system optimized by O'Meara (1999). A Phillips RT 250 (III) Depth Therapy Generator x-ray tube was operated at 250 kVp voltage and 12.5 mA current. The system used a 1 cm thick aluminum polarizer, a 1.6 mm titanium filter placed between the x-ray tube and polarizer, and a 20 cm long copper collimator with 2 cm inner diameter. A 4 mm layer of tin was placed on the front end of the lead shielding box which enclosed the system to reduce the number of lead x-rays which could potentially interfere with the mercury measurements. The system geometry was set up as outlined in section 1.3.3 and diagrammed in figure 1.3.

Measurements were performed using kidney phantoms which consisted of Nalgene® bottles (4.8 cm diameter, 8 cm high) containing aqueous solutions of $HgCl_2$ ranging from 0 to 200 ppm Hg. The phantoms were placed in a water bath at a position of 2 cm lateral depth and 5 cm dorsal depth to simulate the kidney's position in the body. Phantom measurements were 30 minutes live time, with dead time losses of ~ 35 - 40 %. Each measurement was repeated 3 times.

The system used a Princeton Gamma-Tech high purity germanium detector (model NIGP 2020) (active face area 2000 mm^2, thickness 20 mm) operated at a voltage of - 2500 V. A Princeton Gamma-Tech charge-sensitive preamplifier (model RG15B/C) was integral with the detector assembly.

The conventional electronics system consisted of Canberra components: a fast spectroscopy amplifier (model 2024) with a semi-Gaussian shaping time constant of 1.0 μs, a 450 MHz Wilkinson-type ADC (model 8077), and an Accuspec MCA system.

The digital system replaced the conventional amplifier, ADC, and MCA components with the DSA-2000 unit and associated GENIE-2000 software. The shaping parameters for the DSA-2000 were chosen by optimizing the throughput and resolution performance on measurements made using the 200 ppm Hg phantom. Rise times ranging from 1.2 to 2.4 μs, and flat top widths ranging from 0.7 to 1.4 μs were tested. The optimal parameters were chosen as 1.6 μs rise time and 0.9 μs flat top width.

The spectra were analysed using a Marquardt nonlinear least squares fit routine. The spectra were fit in three separate sections: $K_{\alpha 2}$, $K_{\alpha 1}$, and $K_{\beta 1,3}$. The α sections were each fit with single Gaussian peaks, and the β section was fit with two Gaussians. Each section was fit with a single exponential background. The peak intensities found by the Marquardt analyses were plotted against the concentrations of the phantoms. The MDL for each calibration line ($K_{\alpha 2}$, $K_{\alpha 1}$, and $K_{\beta 1,3}$) was determined using the following equation:

$$\text{MDL} = 2 * \sigma \text{ on blank phantom / slope of calibration line}$$

The final MDL for the system was calculated as the inverse variance weighted mean of the three individual calibration lines.

4.2.2 Results

The three calibration curves are shown in Figure 4.1 for the conventional system and in Figure 4.2 for the DSA-2000 system. The α_1 and α_2 calibration curves show better linearity than the $\beta_{1,3}$ curves for both the conventional and DSA-2000 systems due to the greater intensity of the α peaks. The DSA-2000 $\beta_{1,3}$ calibration curve shows better linearity than the conventional system curve, indicating its ability to better process the pulses in the $\beta_{1,3}$ peaks, which are peaks of low intensity sitting on a large background.

The individual and combined MDL's for each system are shown in table 4.1 below.

System	α_1	α_2	$\beta_{1,3}$	Combined
Conventional	31.1 +/- 1.5 ppm	43.9 +/- 3.6 ppm	80.0 +/- 13.3 ppm	24.2 +/- 1 ppm
DSA-2000	23.9 +/- 0.9 ppm	40.3 +/- 3.3 ppm	76.3 +/- 9.8 ppm	19.8 +/- 1 ppm

Table 4.1 Individual and combined MDL's for conventional and DSA-2000 Hg XRF systems.

The combined MDL for the DSA-2000 system is significantly less than that for the conventional system (a reduction of ~ 18 %). The combined MDL for the conventional system is in agreement with the value determined by O'Meara (1999) for the same system set-up and phantom position (26 +/- 1 ppm).

While the use of digital electronics is shown to be an improvement in this polarized XRF system, the system still does not perform as well as expected when compared to the Lund University system described by Börjesson *et al.* (1995). The Lund system employs a 160 kV x-ray generator, 0.35 mm uranium filter, and conventional electronics. At a lateral depth of 7 cm and dorsal depth of 5 cm, this system achieved an MDL of 22 ppm (O'Meara, 1999). The MDL of 24.2 +/- 1 ppm reported in Table 4.1 for the conventional system should have been significantly lower due to the higher voltage (250 kV), different

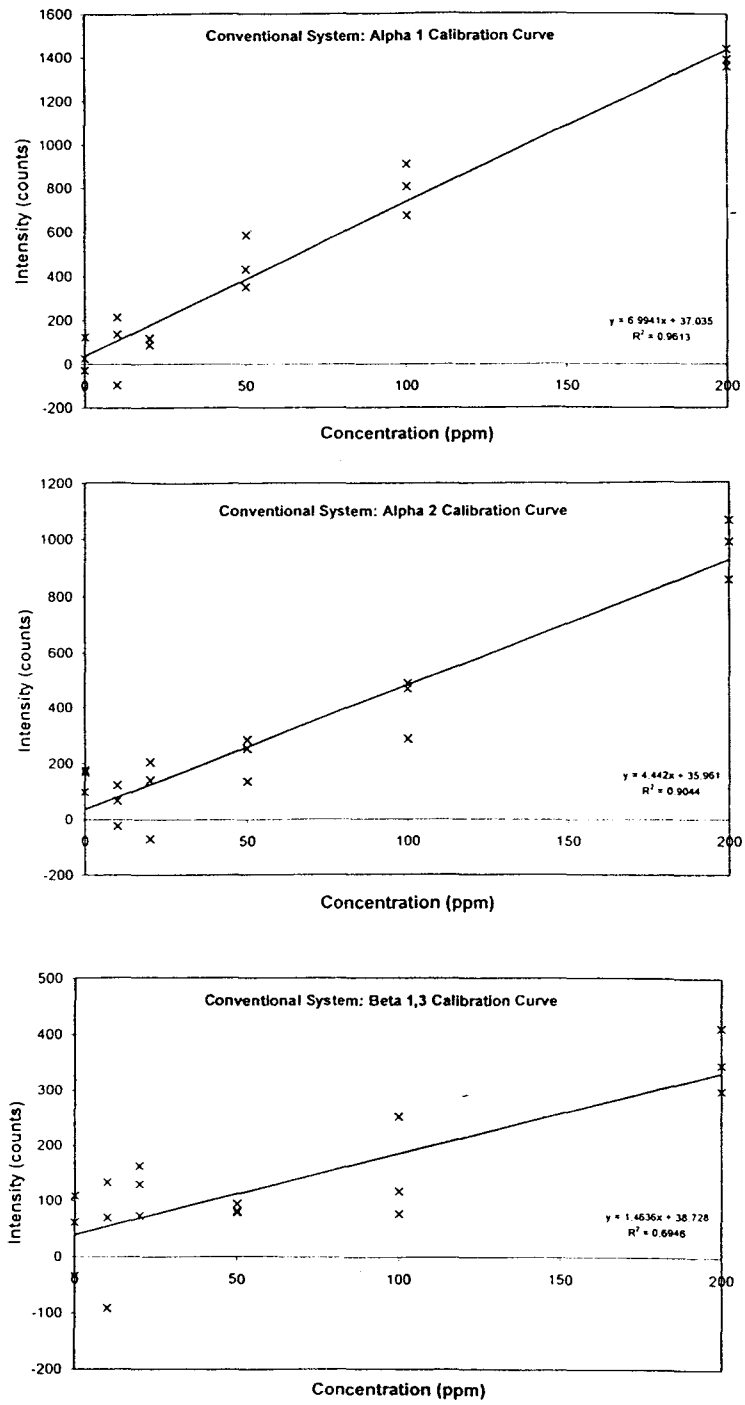

Figure 4.1 Conventional System Hg XRF Calibration Curves

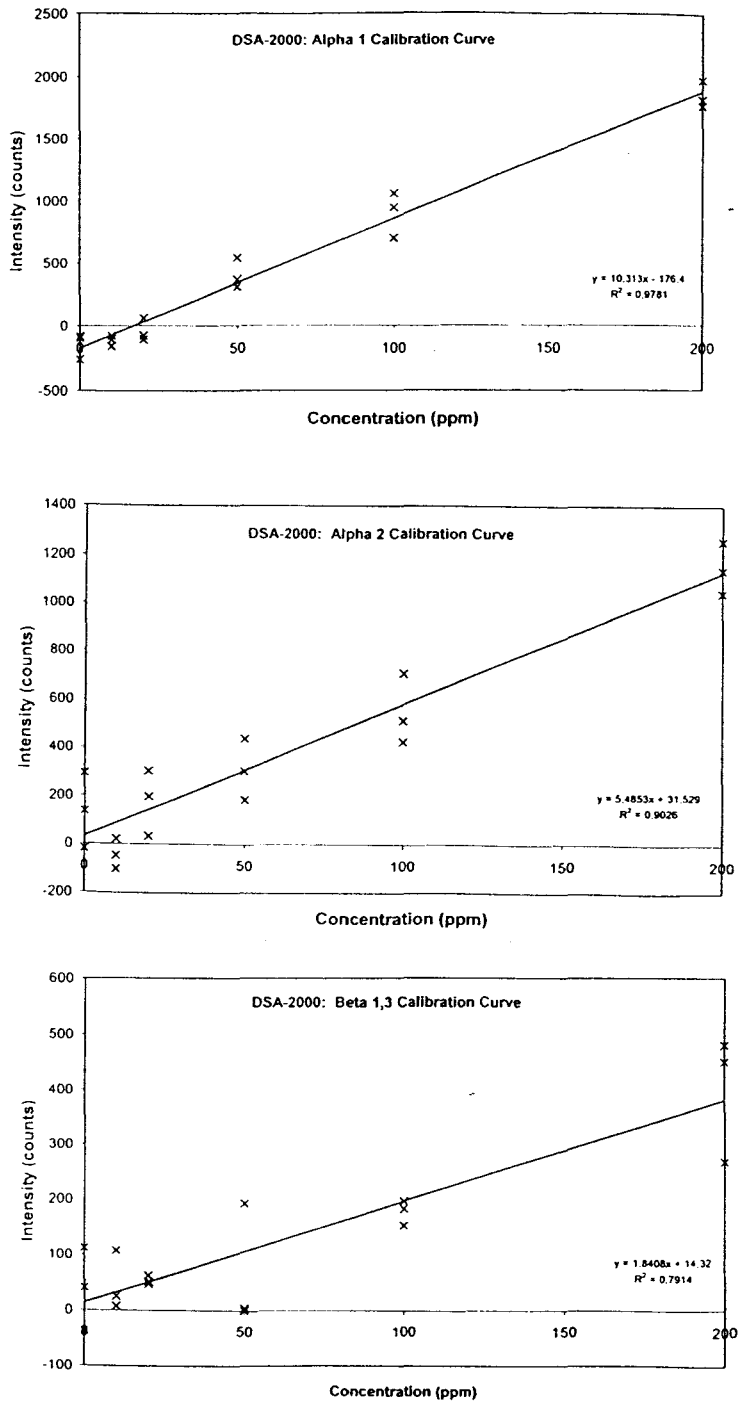

Figure 4.2 DSA-2000 Hg XRF Calibration Curves

filter (1.6 mm titanium), and smaller lateral depth (2 cm). Investigations by O'Meara (1999) determined the effects of these parameters. Increasing the tube voltage from 175 kV to 250 kV (with a 1.6 mm titanium filter, 2 cm lateral and 5 cm dorsal depth) resulted in an MDL decrease by a factor of 1.5 (39 +/- 4 ppm to 26 +/- 1 ppm). Replacing the titanium filter with a 0.3 mm uranium filter (at 175 kV, 2 cm lateral and 5 cm dorsal depth) resulted in an increase in MDL by a factor of 1.6 (39 +/- 4 ppm to 64 +/- 6 ppm). Increasing the lateral depth from 2 cm to 6 cm (at 250 kV, 5 cm dorsal depth, with titanium filter) resulted in an approximate doubling of the MDL. Monte Carlo simulations predicted that a 250 kV, 1.6 mm titanium filter system would result in an MDL reduction by a factor of 3.4 when compared to a 160 kV, 0.35 mm uranium filter system (O'Meara, 1999). While experiments could not be done to test this exact set-up, a comparison between the 250 kV, 1.6 mm titanium system and the 175 kV, 0.3 mm uranium system showed an MDL reduction of 2.5 times (64 +/- 6 ppm to 26 +/- 1 ppm). This lower reduction factor would be expected due to the higher voltage and thicker uranium filter used in the experiments, compared to that used in the simulation.

Overall, the MDL values found using the McMaster system were significantly higher than expected when compared to the Lund results. According to experimental and Monte Carlo predictions, an MDL value of less than 10 ppm should be achievable with a voltage of 250 kV and a 1.6 mm titanium filter. It should be noted that the two systems do differ in data acquisition times (30 minutes live time for the McMaster system, 50 minutes live time for the Lund system) as well as in skin dose rate (1.0 mGy/hr for McMaster's 175 kV, 0.3 mm uranium system compared with 6.0 mGy/hr for Lund's 160

kV, 0.35 uranium system) (O'Meara, 1999). These factors, as well as other possible differences in the x-ray tube or polarizer design may be responsible for the discrepancy in the system performance. If these factors can be determined, and the appropriate changes applied, the combination of increased tube voltage, optimized filtration, and the use of digital spectroscopy will allow for a significant reduction in the current MDL. This improvement will be valuable for the reliable occupational monitoring of kidney mercury levels, and for the study of mercury metabolism by polarized x-ray fluorescence.

Chapter 5

CONCLUSIONS

5.1 Lead

The application of digital spectroscopy systems to the x-ray fluorescence measurement of bone lead has been shown to improve system precision and potentially reduce the minimum detection limit. By having superior pulse processing abilities, the digital spectrometers have much higher fractional throughput than the conventional system, particularly during high count rate situations. The digital systems can maintain high throughput without major losses in resolution, resulting in improved uncertainty in peak area.

Phantom bone lead tests comparing the DSA-2000 digital spectrometer and conventional electronics systems showed a 24.2 % reduction in peak uncertainty for the digital system. This uncertainty improvement translates to a potential reduction in MDL of ~ 1.5 – 2.5 μg Pb/g bone mineral. Phantom tests using a prototype unit of the DSPECplus digital spectrometer resulted in a 7.0 % reduction in peak uncertainty compared to the conventional electronics system. However, phantom measurements made using a commercial DSPECplus unit showed that the performance of the prototype unit was not optimal due to problems with the automatic pole zero functions. It was found that the DSPECplus performance was comparable to that of the DSA-2000, and

would likely also result in an MDL reduction of ~ 1.5 – 2.5 μg Pb/g bone mineral. With the current MDL for the conventional system ranging from about 6 – 10 μg Pb/g bone mineral, and the typical range of normal bone lead levels being approximately 5 – 25 μg Pb/g bone mineral, this potential reduction in MDL is a significant gain. By utilizing the digital systems, the MDL can be brought down to a level below, or near the low end of, the normal lead level range.

Further phantom bone lead tests were done comparing two digital spectroscopy systems (DSPECplus and DSA-2000) and two HpGe detectors (PerkinElmer LOAX and Canberra HpGe). These tests showed that the Canberra HpGe detector and the DSA-2000 digital spectrometer gave the best results for the phantom bone lead measurements. For these tests, the optimal settings for the digital spectrometers were chosen using a merit value method. With the newly optimized settings, the Canberra HpGe – DSA-2000 system showed improvements in measurement precision of 27.4 % compared to conventional electronics. While this improvement is slightly greater than the 24.2 % improvement seen earlier for the DSA-2000, the resulting MDL reduction would still be in the range of ~ 1.5 – 2.5 μg Pb/g bone mineral.

The application of the DSA-2000 spectrometer in the 1999 bone lead survey at Brunswick Mining and Smelting showed superior precision performance for *in vivo* measurements. The median precision value found for calcaneus measurements made using the DSA-2000 was 6.54 μg Pb/g bone mineral, while the median value found for the same individuals using a conventional system in a 1994 survey was 7.82 μg Pb/g bone mineral. The strength of the source was also a contributing factor. For example,

the 1999 calcaneus measurements made using the DSA-2000 and a weaker source (0.3 GBq compared with the 1.3 GBq source used above) resulted in a poorer median precision (8.65 μg Pb/g bone mineral). The best precision performance for *in vivo* bone lead measurements was obtained when a digital spectrometer was used in combination with a high incoming count rate.

Future work in this area could include bone lead tests using other digital spectrometers such as the Digital X-ray Processor (DXP) available from X-ray Instrumentation Associates in California. While this spectrometer offers the same advantage of high throughput with maintained resolution as the digital spectrometers which were tested, it may be designed to suit this specific application better.

The use of digital spectroscopy has been shown to result in improvements in precision and reductions in MDL, in both phantom tests and in *in vivo* XRF bone lead measurements. There are currently other studies underway on improving the lead detection system. Dr. Ian Stronach at McMaster University has determined from Monte Carlo modeling that multi-detector array systems could result in significant improvements in MDL. Results for an integral detector array system consisting of four 8 mm HpGe detectors, each with separate electronics components, show an MDL of 0.36 times the typical MDL for the lead system. Combining these predicted improvements with those found by using digital spectroscopy could potentially result in a four-fold reduction in MDL – a very significant improvement. These improvements in lead detection are very valuable for both the study of lead metabolism, and for the study of the effects of low level environmental lead exposure. As well, the improvements in precision

seen with the digital systems are important for increasing the reliability and measurement range for the occupational and health monitoring of bone lead by x-ray fluorescence.

5.2 Mercury

The application of digital spectroscopy to the polarized x-ray fluorescence measurement of kidney mercury was shown to improve the minimum detection limit of the system. By replacing conventional pulse processing electronics with the DSA-2000 digital spectrometer, the MDL was reduced from 24.2 +/- 1 ppm Hg to 19.8 +/- 1 ppm Hg, an improvement of ~ 18 %. The superior ability of the DSA-2000 to filter the incoming pulses allowed for higher throughput without major losses in resolution, resulting in the MDL decrease. A further reduction in the MDL may be possible by using lower rise time and/or flat top width values with the DSA-2000 spectrometer, allowing for higher throughput with slightly worsened resolution. A merit value method should be used to determine these optimal settings. Future work may also include testing of the mercury kidney system with other digital spectrometers such as the DSPECplus or DXP. As well, trials with a different detector, such as the PerkinElmer LOAX HpGe detector, may result in a further decrease in the MDL of this system.

While the MDL for the conventional kidney mercury system was in agreement with previous results reported by O'Meara (1999), it was significantly higher than expected compared with the findings of Börjesson *et al.* (1995). By increasing the tube voltage and optimizing the filtration, an MDL value lower than 10 ppm should have been achievable. If the discrepancies between the McMaster and Lund systems can be determined, and appropriate adjustments made, significant reductions in MDL are

possible. This improvement will make the *in vivo* polarized XRF measurement of kidney mercury a reliable occupational health monitoring technique, as well as a valuable tool for the study of mercury metabolism.

5.3 Final Remarks

Digital spectroscopy will likely replace conventional electronics pulse processing systems in the future. The digital systems offer a large selection of shaping parameters to suit many applications, they are stable with time and temperature, and their automated computer control makes them easy to operate. More importantly, the digital systems show better fractional throughput performance, improved measurement precision, and reduced minimum detection limits compared to conventional electronics systems. There is even greater potential offered by digital spectroscopy in the future by the possibility of using adaptive filtering. Here, instead of choosing one set of shaping parameters for the entire measurement, the shaping parameters are adapted for each pulse, resulting in the best possible resolution and throughput. These advantages clearly make digital spectroscopy the best choice in pulse processing available today for use in applications such as the x-ray fluorescence measurement of bone lead and kidney mercury.

REFERENCES

Ahlgren, L., Lidén, K., Mattsson, S. and Tejning, S. (1976) X-ray fluorescence analysis of lead in human skeleton *in vivo*. *Scand J Work Environ Health* **2 (2)** 82 - 86.

Akesson, I., Schütz , A., Attewell, R., Skerfving, S. and Glantz, P. (1991) Status of mercury and selenium in dental personnel: Impact of amalgam work and own fillings. *Arch Environ Health* **46 (2)** 102 - 109.

Barregård, L. (1993) Biological monitoring of exposure to mercury vapour. *Scand J Work Environ Health* **19 (suppl 1)** 45 - 49.

Barry, P. S. I. (1975) A comparison of concentrations of lead in human tissues. *Brit J Ind Med* **32** 119 - 139.

Barry, P. S. I. and Mossman, D. B. (1970) Lead concentrations in human tissues. *Brit J Ind Med* **27** 339 - 351.

Bloch, P. and Shapiro, I. M. (1981) An x-ray fluorescence technique to measure the mercury burden of dentists *in vivo*. *Med Phys* **8 (3)** 308 - 311.

Börjesson, J. (1996) Studies of cadmium, mercury, and lead in man: The value of x-ray fluorescence measurements *in vivo*. Ph.D. Thesis, Lund University, Malmö, Sweden.

Börjesson, J., Barregård, L., Sällsten, G, Schütz, A., Jonson, R., Alpsten, M., and Mattson, S. (1995) *In vivo* XRF analysis of mercury: the relation between concentrations in the kidney and the urine. *Phys Med Biol* **40** 413 - 426.

Börjesson, J. and Mattsson, S. (1995) Toxicology; *In vivo* x-ray fluorescence for the assessment of heavy metal concentrations in man. *Appl Radiat Isot* **46** 571 - 576.

Cake, K. (1994) *In vivo* x-ray fluorescence of bone lead in the study of human lead metabolism. M.Sc. Thesis. McMaster University, Hamilton, Ontario.

Canberra (1991) Germanium Detectors: User's Manual. Canberra Industries, Inc., Meriden, Conneticut, U.S.A.

Chettle, D. R., Scott, M. C. and Somervaille, L. J. (1991) Lead in bone: Sampling and quantitation using K x-rays excited by ^{109}Cd. *Environ Health Perspect* **91** 49 - 55.

Christoffersson, J-O and Mattsson, S. (1983) Polarised x-rays in XRF-analysis for improved *in vivo* detectability of cadmium in man. *Phys Med Biol* **28 (10)** 1135 - 1144.

Denny, P., Hart, B.T., Lasheen, M.R., Subramanian, V. and Wong, M.H. (1987) "Group Report: Lead" in: Lead, Mercury, Cadmium and Arsenic in the Environment, Ed. T.C. Hutchinson and K.M. Meema, John Wiley & Sons, Chichester, England.

D'Itri, P. and D'Itri, F. (1977) Mercury Contamination: A Human Tragedy. John Wiley & Sons, New York, U.S.A.

Dzubay, T. G., Jarrett, B. V. and Jaklevic, J. M. (1974) Background reduction in x-ray fluorescence spectra using polarization. *Nucl Instrum Methods* **115** 297 - 299.

Fergusson, J.E. (1990) The Heavy Elements: Chemistry, Environmental Impact and Health Effects. Pergamon Press, United Kingdom.

Fleming, D. (1998) Human lead metabolism: chronic exposure, bone lead and physiological models. Ph.D. Thesis. McMaster University, Hamilton, Ontario.

Fleming, D. E. B., Boulay, D., Richard, N. S., Robin, J-P, Gordon, C. L., Webber, C. E. and Chettle, D. R. (1997) Accumulated body burden and endogenous release of lead in employees of a lead smelter. *Environ Health Perspect* **105 (2)** 224 - 233.

Friberg, L. and Nordberg, G. (1973) "Inorganic Mercury – Toxicological and Epidemiological Appraisal" in: Mercury, Mercurials and Mercaptans, Ed. M. Miller and T.W. Clarkson, Charles C. Thomas, Illinois, U.S.A.

Gerhardsson, L., Attewell, R., Chettle, D. R., Englyst, V., Lundström, N-G, Nordberg, G. F., Nyhlin, H., Scott, M.C. and Todd, A. C. (1993) *In vivo* measurements of lead in bone in long-term exposed lead smelter workers. *Arch Environ Health* **48 (3)** 147 - 156.

Goldberg, E. and Wren, C. (1987) "Group Report – Mercury" in: Lead, Mercury, Cadmium and Arsenic in the Environment, Ed. T.C. Hutchinson and K.M. Meema, John Wiley & Sons, Chichester, England.

Gordon, C. L., Chettle, D. R. and Webber, C. E. (1993) An improved instrument for the *in vivo* detection of lead in bone. *Brit J Ind Med* **50** 637 - 641.

Hall, E.J. (1994) Radiobiology for the Radiologist. J.B. Lippincott Co., Pennsylvania, U.S.A.

Hu, H., Milder, F.L. and Burger, D.E. (1989) X-ray fluorescence: Issues surrounding the application of a new tool for measuring burden of lead. *Environ Res* **49** 295 - 317.

Hutton, M. (1987) "Human Health Concerns of Lead, Mercury, Cadmium and Arsenic" in: Lead, Mercury, Cadmium and Arsenic in the Environment, Ed. T.C. Hutchinson and K.M. Meema, John Wiley & Sons, Chichester, England.

Kaufman, L. and Camp, D. C. (1974) Polarized radiation for x-ray fluorescence analysis. *Adv X-ray Anal* **18** 247 - 258.

Kaye, B. (1995) Science and the Detective. VCH Publishers, Inc., New York, U.S.A.

Knoll, G. F. (1989) Radiation Detection and Measurement, 2nd Edition. John Wiley & Sons, New York, U.S.A.

Landrigan, P.J. (1989) Toxicity of lead at low dose. *Br J Ind Med* **46** 593 - 596.

Langworth, S., Elinder, C-G, Göthe, C-J and Versterberg, D. (1991) Biological monitoring of environmental and occupational exposure to mercury. *Int Arch Occup Environ Health* **63** 161 - 167.

Lederer, C. M. and Shirley, V. S. (1978) Table of Isotopes, 7th Edition. John Wiley & Sons, New York, U.S.A.

Marquardt, D. W. (1963) An algorithm for least-squares estimation of nonlinear parameters. *J Soc Ind Appl Math* **11 (2)** 431 - 441.

Matsuo, N., Suzuki, T., and Hirokatsu, A. (1989) Mercury concentration in organs of contemporary Japanese. *Arch Environ Health* **44 (5)** 298 - 303.

Needleman, H. L. (1977) Exposure to Lead: Sources and Effects. *N Engl J Med* **297 (17)** 943 - 945.

Nierenberg, D.W., Nordgren, R. E., Chang, M. B., Siegler, R. W., Blayney, M. B., Hochberg, R., Toribara, T. Y., Cernichiari, E. and Clarkson, T. (1998) Delayed cerebellar disease and death after accidental exposure to dimethylmercury. *New Engl J Med* **338 (23)** 1672 - 1676.

Nordberg, G. F. and Skerfving, S. (1972) "Metabolism" in: Mercury in the Environment. Ed. L. Friberg and J. Vostal, The Chemical Rubber Company, Ohio, U.S.A.

O'Meara, J. (1999) Measuring Lead, Mercury, and Uranium by *in vivo* X-ray Fluorescence. Ph.D. thesis. McMaster University, Hamilton, Ontario.

Ontario Ministry of Labour. Designated Substances in the Workplace: A Guide to the Mercury Regulation. Occupational Health and Safety Division, Ontario Ministry of Labour, March 1986.

Piotrowski, J. K., Trojanowska, B. and Mogilnicka, E.M. (1975) Excretion kinetics and variability of urinary mercury in workers exposed to mercury vapour. *Int Arch Occup Environ Health* **35** 245 - 256.

Ratcliffe, J.M. (1981) Lead in Man and the Environment. Ellis Horwood Ltd., Chichester, England.

Risher, J. and DeWoskin, R. (1999) Toxicological Profile for Mercury. U.S. Department of Health and Human Services, Public Health Services, Agency for Toxic Substances and Disease Registry, Prepared by Research Triangle Institute, Atlanta, Georgia, U.S.A.

Roels, H., Abdeladim, S., Ceulemans, E. and Lauwerys, R. (1987) Relationship between the concentrations of mercury in air and in blood or urine in workers exposed to mercury vapours. *Ann occup Hyg* **31 (2)** 131 - 145.

Sällsten, G., Barregård, L. and Järvholm, B. (1990) Mercury in the Swedish chloralkali industry – an evaluation of the exposure and preventative measures over 40 years. *Ann Occup Hyg* **34 (2)** 205 - 214.

Sällsten, G., Barregård, L., Langworth, S. and Vesterberg, O. (1992) Exposure to mercury in industry and dentistry: A field comparison between diffusive and active samplers. *Appl Occup Environ Hyg* **7 (7)** 434 - 440.

Schwartz, B. S., Bolla, K. I., Stewart, W., Ford, P., Agnew, J. and Frumkin, H. (1993) Decrements in neurobehavioral performance associated with mixed exposure to organic and inorganic lead. *Am J Epidemiol* **137** 1006 - 1021.

Skerfving, S., Christoffersson, J-O, Schütz, A., Welinder, H., Spång, G., Ahlgren, L. and Mattsson, S. (1987) Biological monitoring, by *in vivo* XRF measurements, of occupational exposure to lead, cadmium and mercury. *Biol Trace Elem Res* **13** 241 - 251.

Skerfving, S., Nilsson, U., Schütz, A. and Gerhardsson, L. (1993) Biological Monitoring of inorganic lead. *Scand J Work Environ Health* **19 (suppl 1)** 159 - 164.

Skerfving, S. and Vostal, J. (1972) "Symptoms and Signs of Intoxication" in: Mercury in the Environment. Ed. L. Friberg and J. Vostal, The Chemical Rubber Company, Ohio, U.S.A.

Smith, J. R.H., Athwal, S. S., Chettle, D. R. and Scott, M C. (1982) On the *in vivo* measurement of mercury using neutron capture and x-ray fluorescence. *Int J Appl Radiat Isot* **33** 57 - 561.

Smith, R.G., Vorwald, A. J., Patil, L. S. and Mooney, T. F. (1970) Effects of the exposure to mercury in the manufacture of chlorine. *Am Ind Hyg Assoc J* **31** 687 - 700.

Somervaille, L. J., Chettle, D. R. and Scott, M. C. (1985) *In vivo* measurement of lead in bone using x-ray fluorescence. *Phys Med Biol* **30 (9)** 929 - 943 .

Todd, A.C., McNeill, F.E., Palethorpe, J.E., Peach, D.E., Chettle, D.R., Tobin, M.J., Strosko, S.J. and Rosen, J.C. (1992) *In vivo* x-ray fluorescence of lead in bone using K x-ray excitation with ^{109}Cd sources: radiation dosimetry studies. *Environ Res* **57** 117 - 132.

Vo, D. T., Russo, P. A. and Sampson, T. E. (1998) Comparisons between digital gamma-ray spectrometer (DSPEC) and Standard Nuclear Instrumentation Methods (NIM) systems. Los Alamos National Laboratory, New Mexico, U. S. A.

Vostal, J. (1972) "Transport and Transformation of Mercury in Nature and Possible Routes of Exposure" in: Mercury in the Environment. Ed. L. Friberg and J. Vostal, The Chemical Rubber Company, Ohio, U.S.A.

Wielopolski, L., Rosen, J. F., Slatkin, D. N., Vartsky, D., Ellis, K. J. and Cohn, S. H. (1983) Feasibility of noninvasive analysis of lead in the human tibia by soft x-ray fluorescence. *Med Phys* **10 (2)** 248 - 251.

Wielopolski, L., Rosen, J. F., Slatkin, D. N., Zhang, R., Kalef-Ezra, J.A., Rothman, J.C., Maryanski, M. and Jenks, S.T. (1989) *In vivo* measurements of cortical bone lead using polarized x rays. *Med Phys* **16 (4)** 521 - 528.

World Health Organization (1977) Environmental Health Criteria 3: Lead. Published under the joint sponsorship of the United Nations Environment Programme and the World Health Organization, Geneva, Switzerland.